Geological Society of America Special Papers

Two anomalies of platinum group elements above the Cretaceous-Tertiary boundary at Beloc, Haiti: Geochemical context and consequences for the impact scenario

Doris Stueben, Utz Kramar, Zsolt Berner, et al.

Geological Society of America Special Papers 2002;356; 163-188
doi:10.1130/0-8137-2356-6.163

Notes

Geological Society of America
Special Paper 356
2002

Two anomalies of platinum group elements above the Cretaceous-Tertiary boundary at Beloc, Haiti: Geochemical context and consequences for the impact scenario

Doris Stüben*
Utz Kramar
Zsolt Berner
Jörg-Detlef Eckhardt
Institut für Mineralogie und Geochemie, Universität Karlsruhe, 76128 Karlsruhe, Germany
Wolfgang Stinnesbeck
Geologisches Institut, Universität Karlsruhe, 76128 Karlsruhe, Germany
Gerta Keller
Department of Geosciences, Princeton University, Princeton, New Jersey, 08544 USA
Thierry Adatte
Institut de Géologie, 11 Rue Emile Argand, 2007, Neuchâtel, Switzerland
Klaus Heide
Institut für Geowissenschaften, Universität Jena, Burgweg 11, 07749 Jena, Germany

ABSTRACT

A detailed geochemical investigation of an expanded Cretaceous-Tertiary (K-T) boundary section near Beloc (B3), Haiti, reveals a complex pattern of sedimentation of multiple origins as a result of erosional, biogenic, volcanic, and impact events. Carbonate-rich uppermost Maastrichtian sediments with high excess rates for Cu, Zn, and Sr (biogenic origin) indicate high productivity ($\delta^{13}C$) and warm temperatures ($\delta^{18}O$). These sediments are overlain by Paleocene (early Danian zone P1a) spherule-rich clayey layers that indicate lower productivity, lower temperatures, and high input of glass and biogenic carbonate. Reworked Maastrichtian sediments are mixed with spherule-rich layers. This spherule-rich deposit is topped by a thin layer rich in Fe that also contains an Ir-dominated anomaly of platinum group elements (PGE) with an almost chondritic abundance pattern, which appears to be the result of a cosmic influx. Monotonous limestones above this interval reflect recovery to normal pelagic sedimentation, which is interrupted by a second PGE anomaly in an Fe-rich clayey layer in the middle part of zone P1a. All PGEs are enriched in this interval and the PGE pattern is basalt like, suggesting a volcanic source. Both PGE anomaly horizons coincide with productivity and temperature changes.

*E-mail: doris.stueben@bio-geo.uni-karlsruhe.de

Stüben, D., Kramar, U., Berner, Z., Eckhardt, J.-D., Stinnesbeck, W., Keller, G., Adatte, T., and Heide, K., 2002, Two anomalies of platinum group elements above the Cretaceous-Tertiary boundary at Beloc, Haiti: Geochemical context and consequences for the impact scenario, *in* Koeberl, C., and MacLeod, K.G., eds., Catastrophic Events and Mass Extinctions: Impacts and Beyond: Boulder, Colorado, Geological Society of America Special Paper 356, p. 163–188.

INTRODUCTION

The origin and genesis of Cretaceous-Tertiary (K-T) boundary sediment layers are still discussed, although most researchers interpret them to be impact derived (Sutherland, 1994; Glasby and Kunzendorf, 1996; Montanari and Koeberl, 2000, and references herein). Central America and the Caribbean play a key role in this debate. In this region, K-T boundary sediments contain glass spherules, shocked quartz, anomalous Ir concentrations (e.g., Alvarez et al., 1980; Officer and Drake, 1985; Bohor and Seitz, 1990; Hildebrand and Boyton, 1990; Hildebrand et al., 1991; Koeberl et al., 1994), and evidence of biotic mass extinction (Maurasse and Sen, 1991; Lamolda et al., 1997; Keller et al., 2001) that are thought to have been generated by a large impact event at Chicxulub in Yucatan, Mexico (Izett et al., 1990; Izett, 1991; Sigurdsson et al., 1991a; Koeberl and Sigurdsson, 1992; Koeberl, 1992; Smit et al., 1992; Kring et al., 1994). According to this scenario, a siliciclastic sequence, which can be intermittently followed over several hundreds of kilometers in northeastern Mexico, was the result of an impact-generated tsunami or gravity flow. Partially altered glass spherules in Mexican and Haitian K-T sediments are interpreted as microtektites or impact glasses, and igneous rocks with andesitic composition in subsurface cores at Chicxulub are considered to be impact melt rocks. A sequence of events is recognized in the K-T boundary transition in the Caribbean area, including an impact, volcanism, and climate and sea-level changes that explain the K-T sediments deposited in the Caribbean area (Keller and Stinnesbeck, 1996; Keller et al., 1997, 2001, this volume; Stinnesbeck et al., 2001).

Stinnesbeck et al. (1999) suggested a multiple-event scenario across the K-T boundary from sections at Beloc, Haiti. Of major interest in these sections is a spherule-rich deposit, which was originally interpreted as a series of volcanogenic turbidites (Maurrasse, 1982). However, geochemical studies revealed that the different layers contain evidence of an impact event (platinum group element [PGE] anomalies, Ni-rich spinels, glass spherules, shocked quartz grains) (Izett et al., 1990, 1991; Izett, 1991; Sigurdsson et al., 1991a, 1991b; Leroux et al., 1995).

Earlier studies of Beloc sections documented a complex sedimentation history, including two Ir enhancements above the spherule-rich deposit, one of them located in an Ir-rich Fe-oxide horizon (Lyons and Officer, 1992; Jéhanno et al., 1992; Leroux et al., 1995). Maurrasse and Sen (1991) and Lamolda et al. (1997) reported the first early Danian species near the top of the spherule layer at 32 cm above the base and 30 cm below the Ir enrichment. Sigurdsson et al. (1991b) reported the first Danian species at 110 cm above the base of the spherule layer, whereas Keller et al. (2001) reported the first Danian species at the base of the spherule layer. The differences in the biostratigraphic results of these reports are primarily due to the localities studied: K-T outcrops along the road are tectonically faulted and sheared and, in consequence, often reduced in thickness. Maurrasse and Sen (1991), Stinnesbeck et al. (2001), and Keller et al. (2001) described outcrops on the steep hillside below the road to Beloc. These outcrops are less affected by faulting and more expanded than the road sections, and provide better age data. This study provides a detailed geochemical and mineralogical investigation of the most complete of these new sections at Beloc, Haiti (section B3), in which two PGE anomalies were reported (Stinnesbeck et al., 1999). Specifically, this study concentrates on the following. (1) A detailed chemostratigraphy study of the Beloc 3 (also known as B3) section was done in order to identify the source and the depositional history of the accumulated material. Special attention is paid to the geochemical discrimination of extraterrestrial, volcanogenic, and terrigenous-detrital signals. (2) A geochemical investigation was made of spherules that accumulated in several layers and their provenance and postdepositional alteration.

ANALYTICAL METHODS

Material and sample preparation

We selected 42 samples for geochemical investigations from an expanded K-T boundary transition at Beloc (Figs. 1 and 2; see Keller et al., 2001, for details of location). Sample locations with the corresponding labels are marked on the lithological profiles by horizontal dashes. The sediment samples were dried, crushed, finely ground, and homogenized in an agate mill and dried at 105°C prior to analysis.

Major and trace elements

Major and trace elements were determined by energy-dispersive (EDXRF) and wavelength-dispersive X-ray fluorescence (WDXRF) analysis. We analyzed 14 trace elements (Ni, Cu, Zn, Ga, As, Rb, Sr, Y, Zr, Nb, Cd, Sb, Ba, and Pb) by EDXRF. For these determinations an aliquot of ~5 g from each of the 42 samples was used as bulk powder in Polystyrol containers with a 6 µm Mylar window for measurement. The samples were measured three times with a SPECTRACE 5000 X-ray analyzer using Al, Pd-, and Cu primary filters to optimize the excitation of elements emitting low, intermediate, and high X-ray energies, respectively. For details of analytical procedures and detection limits for bulk-rock powder samples, see Kramar (1997).

Major elements and some of the minor elements (V, Cr, and Ni) were determined by wavelength-dispersive WDXRF. For these samples fused glass disks were prepared from a mixture of 0.5 g ignited bulk powder, 0.5 g SiO_2, and 4 g SPECTROMELT. The fused disks were analyzed with an SRS 303 AS wavelength-dispersive X-ray spectrometer with Rh-tube excitation. Major elements were evaluated by a fundamental parameter calibration procedure, whereas trace elements were determined using a combined Compton and intensity matrix correction procedure.

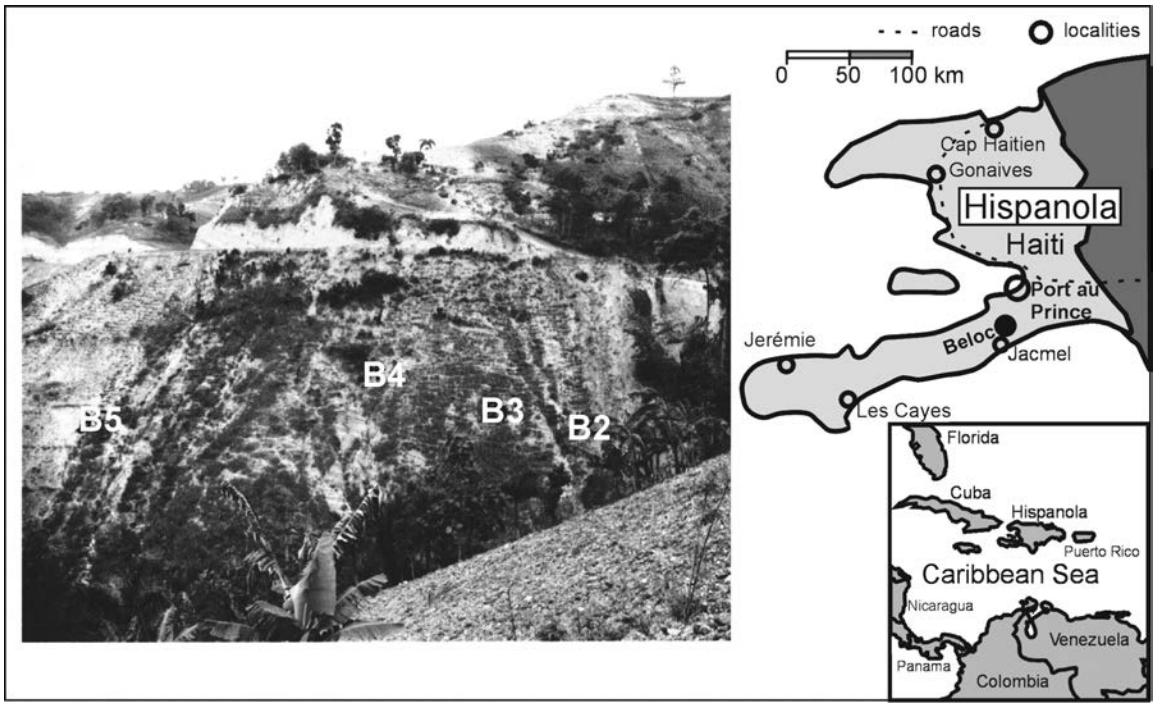

Figure 1. Sketch map of topographic setting of Beloc on island of Haiti and photo of exposed hill slope showing location of Beloc sections B2, B3, and B4 (map is redrawn from Planet Erde multimedia CD, Bertelsmann, 1997, ISBN 3-575-09509-4).

Wavelength-dispersive electron microprobe analyses were conducted by a Cameca SX50 microprobe to determine the main composition of spherules. Accelerating voltage was set to 15–20 kV and counting times of 120–150 s were used. Automatic calibration was performed by means of standard reference minerals. Detection limits are between 500 and 1000 mg/kg. Sulfur contents were evaluated in energy-dispersive mode, detection limits being above 1000 ppm for this element.

Rare earth elements

We selected 10 samples to evaluate the rare earth element (REE) patterns of the bulk material of typical lithological units of the profile. In addition, three samples were prepared of hand-picked spherules consisting of yellowish glass, dark colored glass, and spherules with smectite-like composition, in order to evaluate possible differences in the REE patterns of the different types of spherules in the spherule-rich deposit. After complete digestion with concentrated HF-$HClO_4$(5:1), samples were taken up in HNO_3 (0.15 M). The ratio between sample weight and solution was ~1:1000. Element concentrations were measured by standard inductively coupled plasma-mass spectrometry (ICP-MS) technique (Fisons Plasmaquad 2 turbo+), using an REE multielement standard solution (High-Purity Standard, Charleston, South Carolina) for external calibration and Rh and Bi as internal standards. Analytical accuracy was tested by means of the U.S. Geological Survey Standards SCo-1 (Cody Shale) and SGR-1 (shale). For most elements the measured concentrations are within ±6 relative% of certified values, and precision was better than 3%.

PGEs

We selected 28 samples across the profile for PGE analysis. The very low contents impose a combined procedure of preconcentration and matrix elimination prior to the detection with ICP-MS. This was achieved by fire assay with nickel sulfide collection on parts of thoroughly homogenized samples weighing ~50g. After drying at 105°C, sample material mixed with 30 g of sodium carbonate, 100 g of sodium tetraborate, 10 g of nickel powder, 7.5 g of sulfur and 5–10 g of diatomite was fused for 1 h at 1140°C. The resulting melt segregates by liquation, leading to a Ni-sulfide phase (Ni button or regulus), which collects and concentrates the PGEs. The cooled regulus was crushed and its bulk (NiS) dissolved in concentrated HCl, without attacking the precious metals and their alloys. After filtration through a polytetrafluorethylene (PTFE) membrane filter, the part of the residue containing the PGEs was dissolved in a mixture of hydrogen peroxide and concentrated HCl. Undissolved particles were retained by filtration through a white band quality paper filter. The solution containing the PGEs was slowly evaporated to dryness and taken up with 1% HNO_3 in 10 mL flasks. All chemicals used in the fire-assay step were of reagent grade, those used in the digestion were of suprapure

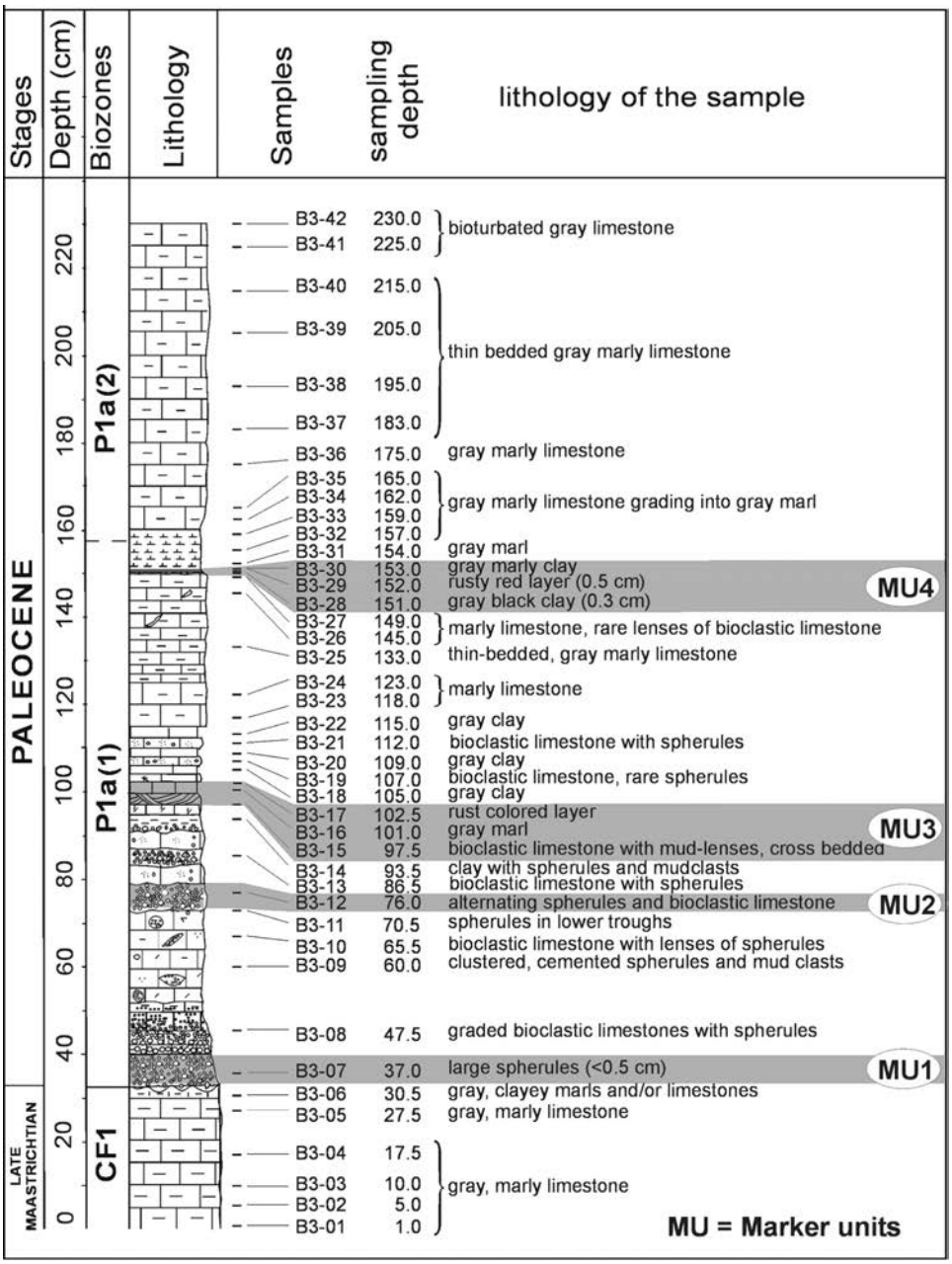

Figure 2. Description of Beloc 3 section giving stratigraphic unit, lithology, sample location, sampling depth, and lithological description of each subsample. (Lithology, stratigraphy, and biozones are redrawn from Stinnesbeck et al., 1999.)

grade. ICP-MS analysis was performed in a similar way as described here, using PGE multielement standard Claritas (SPEX Industries, Grasbrunn, Germany) and Tm and Bi as internal standards.

Accuracy was checked by means of WPR-1 (Canada Centre for Mineral and Energy Technology, CANMET) and SARM-7 (South African Committee for Certified Reference Materials) certified reference materials. The measured contents were found to be within 11% of the certified values, while precision, estimated by the standard deviation of replicate analyses (3σ) was in the range 7%–10%. Based on reference samples analyzed during several years in the lab, recovery was estimated to be better than 85%, which is in the range of the efficiency usually obtained by NiS fire assay (Date et al., 1987; Reddi et al., 1994; Zereini et al., 1994). Detection limits as determined from the average of the blanks were 0.09 ng/g Ir, 0.1 ng/g Rh, 0.4 ng/g Pd, and 0.4 ng/g Pt. These values are mainly dependent on the NiS fire assay; instrumental detection limits of the ICP-MS being approximately two orders of magnitude lower.

Stable isotopes (carbon and oxygen)

Carbon and oxygen isotope ratios in the carbonate fraction of finely ground bulk samples were determined by means of an

automated carbonate preparation system connected on-line to an isotope ratio mass spectrometer (MultiPrep and Optima, both from Micromass UK, Ltd.). The preparation line is based on the standard method by measuring the isotope ratios in CO_2 released by reaction with 100% phosphoric acid. Samples are dissolved in individual vials, eliminating the risk of cross-contamination from one sample to the next, a requirement crucial for accurate and precise isotope ratio measurements on samples as small as <10 µg of calcite. Gas from a CO_2 pressure bottle, calibrated and certified by Messer Griesheim (Germany), was used as reference gas. Instrumental precision was better than 0.008‰ for $\delta^{13}C$ and <0.015‰ for $\delta^{18}O$. Accuracy was checked in each of the analytical batches by running the carbonate standard NBS19. Results were in the range of the certified values within ±‰ for $\delta^{13}C$ and ±‰ for $\delta^{18}O$. Isotope values are reported relative to the Vienna Peedee belemnite (VPDB) standard for both carbon and oxygen.

Bulk-rock mineralogy

For mineralogical characterization of the samples, X-ray diffraction (XRD) analyses on whole-rock samples were carried out. We ground ~5 g of dried rock (60°C) to a homogeneous powder of particle sizes <40 µm (Kübler, 1983). The powdered material (800 mg) was pressed at 20 bar into a powder holder and analyzed by a SCINTAG XRD 2000 diffractometer, using standard semiquantitative techniques based on external standardization (Klug and Alexander, 1974; Kübler, 1983, 1987).

Degassing experiments

For the degassing experiments glass spherules were separated by hand-picking under binocular (samples B3–7 and B3–12). The sample weight (10–30 mg, representing 10–20 spherules) is limited with respect to the degassing rate and the content of volatiles. The evolved gas analyses (EGA) were carried out using high-temperature mass spectrometry as described in detail in Heide (1974) and Stelzner and Heide (1996). The degassing process occurs far from equilibrium conditions. Reverse reactions between the volatiles and the melt thus cannot occur. The samples are heated under vacuum of 10^{-4} Pa to 10^{-3} Pa at a rate of 10 K/min to 1500°C; hence interactions between the evolved gases were minimized and a determination of the primary volatile species is possible. Turbomolecular pumps are used to eliminate hydrocarbons in the background of the vacuum devices. Analyses of the volatiles were carried out using a quadrupol mass spectrometer (QMA 125, Balzers) operated in rapid scan mode or in a multiple ion detection mode during the entire heating period. The measurements yield ion currents at distinct mass numbers (m/z 1–100; at a mass resolution of ~1 amu), which are proportional to the partial pressure of the various volatiles escaping from the melt during the heat treatment. Fragmentation of molecules occurs during ionization in the ion source of the mass spectrometer. Isotopic abundances and background contributions were taken into consideration for the interpretation of the gas release curves. To test the system background before and after a cycle, measurements were carried out in a blank experiment (i.e., degassing profiles of the equipment without samples). Detection limits depend on sample size and gas species; herein 0.1–1 ppm for CO_2 and SO_2 and ~100 ppm for H_2O.

GEOLOGICAL SETTING AND LITHOLOGY

The Beloc 3 (B3) section is located ~1 km north of Beloc (Fig. 1) on a steep slope, 20–30 m below the road. More than 100 m of Late Cretaceous and 30 m of Danian deposits are horizontally layered and exposed along this hillslope. The B3 section analyzed for this study includes 30 cm of latest Maastrichtian sediments, the K-T boundary, and 200 cm of Paleocene sediments (Stinnesbeck et al., 2001) (Fig. 3). Latest Maastrichtian pelagic marly limestones contain radiolarians, calcispheres, sponge spicules, ostracods, benthic foraminifera, and abundant planktic foraminifera and disconformably underlie spherule-rich deposits. An undulating erosional surface characterizes the lithological contact that separates the spherule-rich deposit from the latest Maastrichtian pelagic marly limestone. The spherule-rich deposit contains abundant evidence of reworked sediments, such as subrounded clasts of limestone, mudstone, and wackestone, some of which contain reworked early late Maastrichtian planktic foraminifera. The K-T boundary is placed at the disconformity at the base of the spherule-rich deposit based on the abundant presence of Danian planktic foraminifera in the spherule-rich deposit (Keller et al., 2001). Maurrasse and Sen (1991) and all other authors also place the K-T boundary at the lithological change between the limestones and the base of the spherule-rich deposit.

The spherule-rich deposit (30–100 cm) consists of 11 lithologically distinct layers (Stinnesbeck et al., 2001). These layers are characterized by changes in abundance of spherules and bioclastic debris and are separated by erosional contacts and reworking, as indicated by grain-size gradation and erosional disconformities. Four distinct lithological units (marker units, MU) can be recognized within the section, and these are interlayered with marls or marly limestones (Fig. 3). MU1 forms the basal 10–20 cm of the spherule-rich deposit just above the previously defined K-T boundary and is characterized by abundant spherules altered to blocky calcite and smectite. MU2 is located 70–80 cm upsection and is characterized by the presence of abundant black glass spherules with altered rims (to ~60%–70% relative abundance), visible with the naked eye in the outcrop. MU3 is near the top of the spherule-rich deposit at 100–102 cm from the base, and consists of a 2-cm-thick gray-green shale containing a thin rust-colored layer. MU4 is 150 cm above the base of the spherule-rich deposit and is marked by a rust-colored layer associated with volcanic ash between layers of micritic limestone rich in pelagic microfossils (e.g.,

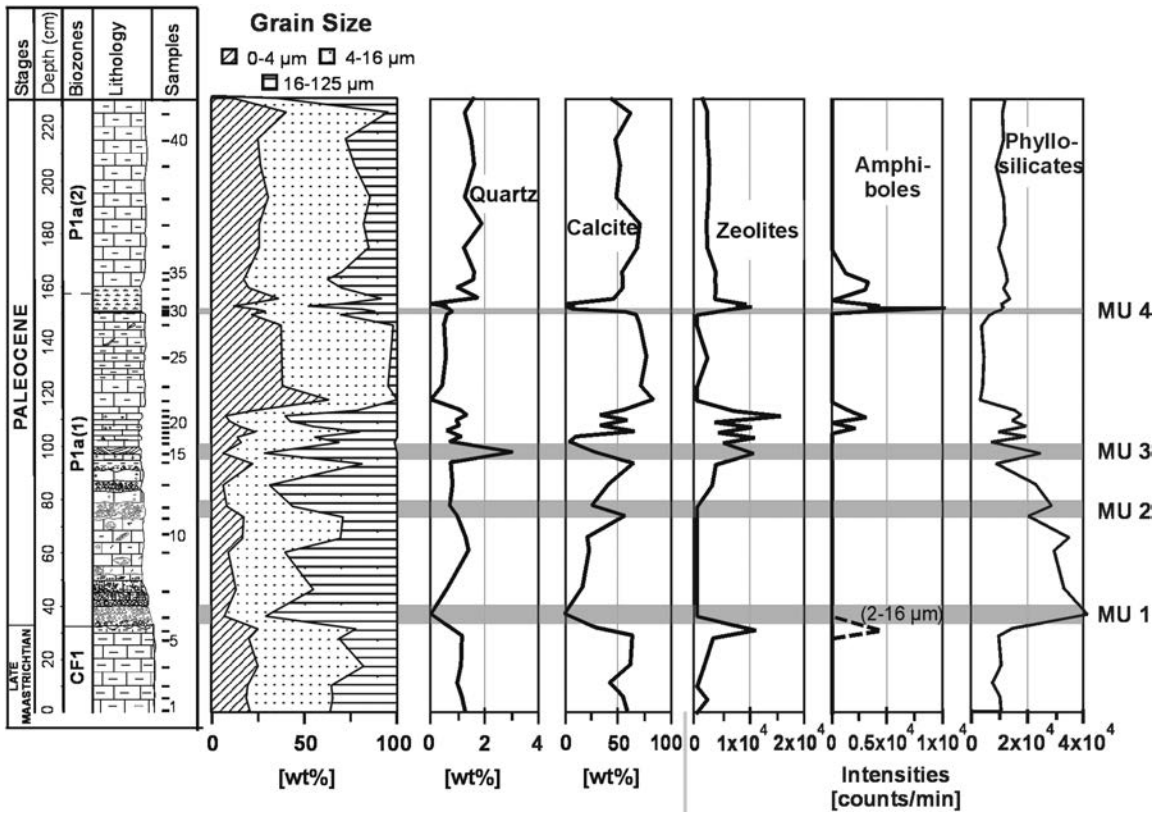

Figure 3. Stratigraphy of Beloc B3 Cretaceous-Tertiary (K-T) section showing grain size, quartz, calcite, zeolite, amphibole, and phyllosilicate distribution. (Lithology, stratigraphy, and biozones are redrawn from Stinnesbeck et al., 1999.)

planktic foraminifera and the calcareous nannofossil *Thoracosphaera*).

RESULTS AND DISCUSSION

Mineralogical results

Bulk-rock data of the Beloc section indicate that normal pelagic conditions dominated by biogenic calcite and low detrital quartz characterize the Maastrichtian (Fig. 3). A possible volcanic pulse is indicated in the uppermost Maastrichtian sediment layer (sample B3–6), as suggested by the presence of amphiboles (hornblende, basaltic type) and increased amount of zeolite (heulandite-clinoptilolite and phillipsite). Basaltic hornblende occurs in a large variety of volcanic rocks varying in composition from basalts to trachytes (Deer et al., 1992). Kring et al. (1994) interpreted hornblende in K-T boundary sediments at Beloc as reflecting a direct volcanic input or the erosion of volcanic rocks. Phillipsite predominates in volcanogenic and clayey sediments, as a diagenetic alteration product of basaltic glass (Kastner and Stonecipher, 1978). At Beloc, clinoptilolite is present throughout the section and derives either from chert and/or opal, or from alteration of basaltic glass (Hataway and Sachs, 1965; Weaver, 1968). The occurrence of zeolites (clinoptilolite and harmotome) at Beloc was reported by several authors in connection with altered glass spherules (Lyons and Officer, 1992; Jéhanno et al., 1992; Bohor and Glass, 1995), but note that maxima in hornblende coincide with high zeolite and smectite contents, suggesting that zeolites (especially phillipsite) mainly derive from alteration of basaltic volcanic material. There is no doubt that the smectite rinds around the glass cores of spherules are a direct alteration product of the spherule glass. However, the mineral association zeolite, smectite, and amphibole, characteristic for several distinct layers (e.g., at 30 cm in the topmost part of the Maastrichtian, at 10–20 cm above MU3, and in MU4) is not always associated with spherules in this section. Consequently, smectites and zeolites are not necessarily an alteration product of the spherules (Bohor and Glass, 1995), but could also be indicative of episodic volcanic inputs throughout the section.

The spherule-rich layers within the spherule-rich deposit (MU1 and MU2) are generally characterized by a high amount of phyllosilicates (mostly smectite, which is probably derived from glass alteration), variable calcite, and low quartz content. The absence of significant detrital input into these layers is consistent with an interpretation of reworked particles (e.g., spherules, glass, planktic foraminifera) derived from a pelagic environment (e.g., upper slope), rather than intensive erosion of an adjacent emergent area.

MU3 and MU4, which are characterized by significant PGE anomalies (see following) are rich in zeolites and MU4 may coincide with a volcanic influx, as indicated by a high amphibole content. The marly limestone layers located between the two PGE anomalies show mineralogical assemblages dominated by high calcite, and reflect normal pelagic conditions.

A volcaniclastic contribution was also observed by Jéhanno et al. (1992) and Leroux et al. (1995) in their Beloc section ~70–80 cm above the spherule-rich deposit and in association with shocked minerals and an Ir anomaly of 28 ng/g. Revisiting the Beloc section of Maurrasse and Sen (1991) and Lamolda et al. (1997), we found hornblende and increased zeolite abundances in the upper part of the section in association with their reported Ir anomaly.

Major and trace elements

Concentrations of major and trace elements in the Beloc K-T section show considerable variations that indicate fluctuation in the source and nature of the deposited materials, and may also reflect postdepositional changes (Tables 1 and 2). The geochemistry of marine sediments depends on a series of factors, the most important being the biogenic particle flux (productivity) and terrigenous flux. The latter represents a mixture of wet-deposited and eolian-transported material, downslope clastic input near continental margins, volcaniclastic and hydrothermal flux in areas with volcanic activities, and accumulation of authigenic phases. High productivity results in accumulation of biogenic carbonate, opal, and C_{org} dominated sediments (Leinen et al., 1986). Calcium, Mg, Sr, and Cd are incorporated into biogenic carbonate. Manganese, traces of other metals (e.g., V, Mo), and REEs tend to be adsorbed onto organic matter. The major parts of Ti, Al, Cr, K, and Fe are bound in the lattices of minerals of terrigenous debris (Murray and Leinen, 1993). Within this group Ti is by far the most immobile element during weathering (Schroeder et al., 1997). The small amount of Ti involved in the biogeochemical cycle (Orians et al., 1990) is negligible. Authigenic phases (e.g., zeolites, authigenic carbonates, manganese coatings, and hydrogenous phases) play an important role in the accumulation of trace metals in sediments. The major part of Ba is removed from the water column by precipitation as sulfate and is enriched at continental margins (Torres et al., 1996). Alteration can lead to a considerable redistribution of the elements, but it is generally restricted to the volcanogenic material, and is less important in the more resistant detrital components and in authigenic phases that are generally in equilibrium with the depositional environment. Postburial diagenesis is unlikely to change the ratio between the accumulated metals, although it may redistribute some of the trace elements among the different mineral phases on a local scale (Leinen and Stakes, 1979).

CaO is the main component for biogenic carbonate sedimentation and varies from 4 wt% (in layers dominated by clays and terrigenous and/or volcanic material) to 50 wt% (nearly pure calcite) with a clear negative correlation to Zr and TiO_2 (Fig. 4). Because Zr and Ti are nearly immobile during weathering or diagenetic alteration (e.g., Barkatt et al., 1984; Zielinski, 1982, 1985) and are introduced into the sediments exclusively by detrital accumulation, they can be used as proxies for the amount of terrigenous and/or volcanogenic components within the sediment.

From the base of the section to the paleontologically defined Maastrichtian-Paleocene boundary at 30 cm (Keller et al., 2001), CaO concentrations in the marly limestones decrease slightly (from ~35 to 25 wt%). Zirconium and TiO_2 contents (Fig. 4) remain nearly constant at low levels (average 27 µg/g Zr; 0.2 wt% TiO_2), indicating a very low and approximately constant terrigenous component in the sediment during the latest Maastrichtian. Within the spherule-rich layer of MU1, Zr and TiO_2 concentrations increase (~70 µg/g Zr; ~0.4 wt% TiO_2), whereas the Rb content decreases from 10 to 2 µg/g. These elements remain relatively constant in the interval from 30 to 65 cm. CaO also shows constant values of ~20 wt% in this interval, except for one sample at 35 cm, where the value drops to 5 wt% (Fig. 4). In general, this part of the section is less carbonate rich than the late Maastrichtian, but shows the highest phyllosilicate content (Fig. 4).

In the upper part of the spherule-rich deposit (65–100 cm), these elements display rapidly changing compositions of a factor of 2 for CaO and Zr, indicating abrupt changes in the sediment mineralogy (increasing calcite to the detriment of phyllosilicates). These rapid changes can be explained by reworking and redeposition of older Maastrichtian sediments within the early Danian. At 102 cm, MU3 contains a thin, rust-colored Fe-rich layer (to 19 wt% Fe_2O_3; Fig. 4) enriched in most of the trace elements examined (e.g., TiO_2, Zr, Ni, Cu, Zn, Cd, Sn, and Sb), and very low in CaO (~5 wt%) (Figs. 4 and 5). This rust-colored layer is overlain by a 50-cm-thick marly limestone, which is low in TiO_2, Zr, Rb, Cu, Zn, Sn, and Sb, and indicates very low terrigenous input and high carbonate accumulation.

Dark gray clay and a second Fe-rich horizon (to 20 wt% Fe_2O_3) are observed between 150 and 152 cm (MU4). These layers are clearly enriched in Cu, Zn, Ni, As, Pb, Cd, and Sb (Fig. 5). Compared with the marly limestone between the two rust-colored layers, the marls overlying the dark gray clays of MU4 (152–239 cm) show higher concentrations of terrigenous or volcanic materials (e.g., Rb, Zr, and Ti). Rubidium content increases continuously and Ti and Zr increase slightly upsection.

Strontium content varies from 96 to 950 µg/g within the section, whereas Ba ranges from 200 to 6500 µg/g. Within the Beloc section, Ba shows very low concentrations (~200 µg/g) in the marly limestone of the latest Maastrichtian, whereas Sr displays intermediate concentrations (500–600 µg/g). Both elements are evidently enriched (950 µg/g Sr and 6455 µg/g Ba) at the Maastrichtian-Paleocene boundary. The overlying spherule-rich layers and bioclastic limestones (30–100 cm above the base) are lower in Sr (200–300 µg/g) and higher in

TABLE 1. MAJOR ELEMENT COMPOSITION OF BULK SAMPLES

Sample #	Sampling depth (cm)	Na_2O (wt%)	MgO (wt%)	Al_2O_3 (wt%)	SiO_2 (wt%)	P_2O_5 (wt%)	CaO (wt%)	K_2O (wt%)	TiO_2 (wt%)	MnO (wt%)	Fe_2O_3* (wt%)	LOI (wt%)	Total (wt%)
BE3-42	230	0.33	2.15	4.69	34.32	0.17	30.07	0.62	0.30	0.04	2.99	25.63	101.33
BE3-41	225	0.30	1.79	4.07	42.03	0.14	27.09	0.55	0.26	0.03	2.81	23.04	102.12
BE3-40	215	0.38	2.10	4.87	33.42	0.15	28.89	0.67	0.34	0.07	3.57	24.91	99.36
BE3-39	205	0.34	1.85	4.72	31.10	0.13	31.80	0.57	0.30	0.04	3.12	27.01	100.99
BE3-38	195	0.24	1.39	3.74	16.27	0.09	40.47	0.41	0.22	0.08	2.21	33.21	98.34
BE3-37	183	0.23	1.69	3.92	20.69	0.12	38.15	0.44	0.23	0.08	2.53	32.32	100.39
BE3-36	175	0.26	1.43	3.82	17.29	0.10	40.66	0.48	0.24	0.08	2.04	31.96	98.36
BE3-35	165	0.32	2.04	5.12	23.20	0.12	35.50	0.63	0.30	0.06	3.16	29.79	100.24
BE3-34	162	0.33	2.12	5.54	23.30	0.11	34.51	0.70	0.32	0.05	3.08	29.05	99.10
BE3-33	159	0.32	2.27	5.60	25.08	0.17	33.96	0.65	0.31	0.05	3.50	29.26	101.18
BE3-32	157	0.35	3.15	7.01	29.61	0.13	30.01	0.68	0.35	0.03	3.78	25.50	100.60
BE3-31	154	0.36	3.46	7.71	32.94	0.12	27.63	0.65	0.35	0.03	4.15	23.79	101.20
BE3-30	153	0.79	5.87	13.20	51.13	0.08	8.45	0.43	0.51	0.01	11.09	8.18	99.75
BE3-29	152	1.05	3.33	11.09	41.83	0.12	7.92	0.33	0.50	0.07	18.91	9.03	94.17
BE3-28	151	0.32	2.16	5.97	27.26	0.11	31.40	0.51	0.31	0.05	3.75	26.81	98.63
BE3-27	149	0.08	0.98	1.69	18.20	0.10	42.88	0.15	0.11	0.07	1.20	35.58	101.05
BE3-26	145	0.07	0.66	1.08	8.42	0.06	49.52	0.14	0.07	0.10	0.67	39.64	100.43
BE3-25	133	0.11	0.97	1.74	9.85	0.08	47.03	0.22	0.13	0.08	1.09	37.72	99.01
BE3-24	123	0.05	0.70	0.90	5.90	0.05	49.14	0.11	0.06	0.09	0.71	39.74	97.47
BE3-23	118	N.D.	N.D.	N.D.	N.D.	N.D.	N.D.	N.D.	N.D.	N.D.	N.D.		
BE3-22	115	0.08	1.17	2.57	15.37	0.05	44.21	0.18	0.12	0.08	1.37	35.78	100.98
BE3-21	112	0.17	1.85	5.17	25.28	0.06	35.07	0.23	0.17	0.04	2.25	30.48	100.78
BE3-20	109	0.13	2.18	4.51	20.85	0.06	37.96	0.20	0.17	0.05	2.14	32.55	100.81
BE3-19	107	0.09	3.44	6.77	33.03	0.05	28.87	0.25	0.31	0.01	4.17	24.94	101.94
BE3-18	105	0.07	1.54	3.29	15.56	0.08	41.99	0.21	0.11	0.06	1.12	35.59	99.62
BE3-17	102.5	0.05	2.88	6.90	39.40	0.05	10.38	0.21	0.45	0.03	15.88	23.37	99.62
BE3-16	101	0.10	2.84	5.80	28.27	0.08	30.90	0.37	0.25	0.06	2.52	27.75	98.93
BE3-15	97.5	0.06	4.37	7.22	33.31	0.02	16.95	0.21	0.35	0.03	4.35	32.90	99.77
BE3-14	93.54	0.11	3.57	6.32	28.82	0.07	28.08	0.34	0.21	0.04	2.55	31.12	101.24
BE3-13	86.5	N.D.	N.D.	N.D.	N.D.	N.D.	N.D.	N.D.	N.D.	N.D.	N.D.	N.D.	
BE3-12	76	0.03	6.00	6.58	30.78	0.04	25.78	0.10	0.26	0.09	5.01	25.08	99.76
BE3-11	70.5	0.04	4.78	5.84	27.05	0.04	31.25	0.15	0.25	0.04	3.96	27.38	100.79
BE3-10	65.5	0.04	7.35	9.36	42.10	0.02	16.65	0.16	0.39	0.01	6.31	18.38	100.78
BE3-09	60	0.04	6.37	8.99	43.29	0.02	15.69	0.18	0.45	0.03	6.70	18.28	100.02
BE3-08	47.5	<0.02	8.09	11.72	50.26	0.02	10.74	0.13	0.52	0.01	7.77	14.25	103.53
BE3-07	37	N.D.	8.26	11.72	51.00	0.01	5.30	0.10	0.53	0.04	7.96	10.82	95.74
BE3-06	30.5	0.54	3.20	10.16	45.02	0.11	19.82	0.58	0.49	0.03	3.76	18.20	101.93
BE3-05	27.5	0.28	1.56	3.58	23.96	0.13	36.59	0.45	0.25	0.07	2.42	30.71	100.00
BE3-04	17.5	0.21	1.00	2.49	46.81	0.07	26.96	0.32	0.19	0.03	1.70	21.76	101.54
BE3-03	10	N.D.	N.D.	N.D.	N.D.	N.D.	N.D.	N.D.	N.D.	N.D.	N.D.	N.D.	
BE3-02	5	0.25	1.28	3.09	26.31	0.10	36.28	0.37	0.21	0.06	2.10	30.00	100.08
BE3-01	1	0.25	1.50	3.26	31.69	0.09	33.77	0.42	0.23	0.06	2.22	27.23	100.72

Note: Major element composition and LOI of the bulk samples determined by Wavelength Dispersive X-ray Fluorescence spectrometry (WDXRF). Concentrations of major elements in the Beloc Cretaceous-Tertiary section B3 show considerable variations, which primarily indicate fluctuation in the source and nature of the deposited materials, but may also reflect postdepositional changes.
*All Fe as Fe_2O_3
N.D. = not determined; LOI = loss on ignition.

Ba concentrations (450–800 mg/g) than the Maastrichtian marly limestone. The two rust-colored layers of MU3 and MU4 and adjacent clays are enriched in both elements (to 920 mg/g Sr and 6000 µg/g Ba) (Fig. 4). Above the gray clay of MU4, Sr and Ba contents decrease gradually to the top of the section. Barium shows a strong and Sr a moderate positive correlation to Zr and TiO_2 in the interval above 90 cm (Fig. 4).

The abundances of Sr and Ba in sediments are controlled by various factors, including terrigenous influx, biogenic flux, hydrothermal input, and sedimentation rates (Schroeder et al., 1997). To evaluate the part of the elements bound to the diffuse terrigenous component, the so-called excess concentrations of various elements (El*) were calculated (Murray and Leinen, 1993, 1996; Schroeder et al., 1997). Assuming the same element to Ti ratio in the sample as in a representative reference material, a theoretically expected content for each element can be calculated. The excess concentration (El*) is the deviation between the actually found content and the expected concentration of the respective element:

$$El^* = El_{total} - [Ti_{sample}^* (El_{NASC}/Ti_{NASC})], \quad (1)$$

where El_{total} is the bulk concentration of the element; Ti_{sample}, the concentration of Ti in the sample; El_{NASC} and El_{PAAS} are the concentrations of the element in the NASC (North Ameri-

TABLE 2. MINOR ELEMENT CONTENTS AND STABLE ISOTOPE DATA OF BULK SAMPLES

Sample #	Sampling depth (cm)	Cr (μg/g)	Ni (μg/g)	Cu (μg/g)	Zn (μg/g)	As (μg/g)	Rb (μg/g)	Sr (μg/g)	Y (μg/g)	Zr (μg/g)	Nb (μg/g)	Ba (μg/g)	Pb (μg/g)	$\delta^{13}C$ ‰ VPDB	$\delta^{18}O$ ‰ VPDB
BE3-42	230	48	32	83	101	3	20	619	35	91	3	1993	<5	−0.27	−4.00
BE3-41	225	47	32	59	60	<3	16	561	22	79	<2	1199	<5	0.11	−3.41
BE3-40	215	51	35	73	90	3	20	612	24	90	3	2547	<5	−0.45	−3.73
BE3-39	205	47	28	81	84	<3	15	655	27	94	3	2011	<5	−0.39	−3.24
BE3-38	195	62	34	61	66	<3	12	734	33	85	10	1579	<5	−0.17	−2.75
BE3-37	183	37	26	46	68	<3	14	639	33	92	<2	1508	<5	0.41	−1.48
BE3-36	175	72	29	57	66	<3	14	760	34	89	13	1715	<5	0.27	−1.41
BE3-35	165	68	35	89	110	3	17	800	29	97	12	3000	7	0.04	−1.98
BE3-34	162	56	34	77	114	3	24	752	41	110	7	2792	<5	−0.42	−2.61
BE3-33	159	50	35	70	97	3	18	750	37	105	4	3000	<5	−0.21	−1.78
BE3-32	157	73	55	72	87	<3	22	763	13	108	13	3093	<5	−1.46	−1.83
BE3-31	154	53	58	77	84	<3	15	784	17	109	10	3899	<5	−0.86	−1.75
BE3-30	153	29	103	105	149	8	10	666	4	116	10	5273	7	−1.68	−1.19
BE3-29	152	54	209	145	152	21	7	792	5	62	4	5479	12	−0.37	−2.83
BE3-28	151	73	42	60	80	<3	14	865	17	97	12	5371	<5	0.39	−2.08
BE3-27	149	25	15	32	50	<3	6	618	11	81	<2	796	<5	0.71	−0.82
BE3-26	145	30	20	21	36	N.D.	6	630	9	66	<2	690	<5	0.74	−0.93
BE3-25	133	58	25	33	42	<3	10	663	13	69	3	941	<5	0.86	−1.06
BE3-24	123	37	16	22	29	<3	7	683	11	67	<2	452	<5	0.77	−0.62
BE3-23	118	N.D.	N.D.	15	18	<3	N.D.	N.D.	0	N.D.	N.D.	410	<5	0.64	−0.69
BE3-22	115	38	20	20	37	<3	7	735	18	81	4	1305	<5	0.42	−0.77
BE3-21	112	57	21	N.D.	N.D.	N.D.	7	889	12	109	3	N.D.	N.D.	−0.15	−0.78
BE3-20	109	46	31	23	48	<3	4	617	12	94	<2	1400	<5	−0.50	−0.93
BE3-19	107	59	47	35	73	<3	12	955	2	118	3	2181	<5	−0.56	−2.16
BE3-18	105	47	19	20	32	<3	5	632	17	84	N.D.	1285	<5	−1.04	−1.16
BE3-17	102.5	53	103	41	97	49	11	754	N.D.	98	N.D.	2017	16	−0.27	−3.75
BE3-16	101	40	34	29	45	<3	7	701	N.D.	92	<2	2642	<5	−0.29	−1.97
BE3-15	97.5	40	38	32	89	<3	3	557	3	114	<2	5939	6	−1.05	−3.77
BE3-14	93.5	45	23	20	33	<3	9	706	20	112	3	1463	<5	−0.49	−1.12
BE3-13	86.5	N.D.	N.D.	73	90	3	N.D.	N.D.	0	N.D.	N.D.	2547	<5	−0.21	−2.06
BE3-12	76	32	23	22	30	<3	<2	324	9	82	<2	584	<5	−5.05	−4.06
BE3-11	70.5	56	25	19	22	<3	<2	392	6	86	<2	671	<5	−1.72	−1.41
BE3-10	65.5	42	25	22	31	<3	5	213	2	89	4	466	<5	−5.65	−4.03
BE3-09	60	39	25	20	24	<3	11	261	N.D.	94	<2	876	<5	−0.09	−1.64
BE3-08	47.5	40	42	24	30	<3	4	191	N.D.	97	2	854	6	−4.95	−3.77
BE3-07	37	38	82	21	43	<3	6	140	N.D.	93	3	1457	<5	−3.34	−1.16
BE3-06	30.5	61	33	50	60	<3	19	1154	12	130	11	6455	<5	−0.37	−2.51
BE3-05	27.5	51	20	N.D.	N.D.	N.D.	13	711	34	93	<2	N.D.	N.D.	0.56	−2.09
BE3-04	17.5	45	24	39	51	<3	11	610	11	54	4	194	<5	1.53	−2.71
BE3-03	10	N.D.	N.D.	51	64	N.D.	N.D.	N.D.	0	N.D.	N.D.	326	<5	1.25	−3.02
BE3-02	5	N.D.	N.D.	55	69	<3	N.D.	N.D.	0	N.D.	N.D.	435	<5	0.64	−2.04
BE3-01	1	57	28	49	117	<3	14	726	19	75	9	384	<5	1.46	−2.09

Note: Minor element contents and stable isotope data of the bulk samples (minor elements determined by Energy Dispersive X-ray Flourescence [EDXRF] and Wave Dispersive X-ray Flourescence [WDXRF] and C and O isotopes by Isotope Ratio Mass Spectrometry). The minor element contents show considerable variations, which primarily indicate fluctuation in the source, reworking, and primary productivity. C and O isotopes mainly reflect climatic changes.
N.D. = not determined; VPDB = Vienna Peedee belemnite.

can Shale Composite) and the PAAS (Post-Archaean Average Australian Shale), respectively, and Ti_{NASC} is the concentration of Ti in NASC. Because the eolian input in the Caribbean originates mainly from North America, data for the NASC (Gromet et al., 1984) were used instead of PAAS (Taylor and McLennan, 1985), except where no NASC data were available (e.g., for Cu and Zn).

To allow an easier comparison of the excess concentrations of different elements, the ratio of excess to bulk concentrations were calculated:

$$R_{El} = El^*/El_{total}. \quad (2)$$

This ratio expresses the relative amount of an element that is not bound to the detrital components of the sediment. Accuracy of the estimates depends on the composition of the local terrestrial rocks, which were exposed to weathering, but variations in the average composition of the source rocks are probably much lower than the variations observed within the Beloc section.

The El^*/El_{total} ratios for Cu, Zn, Sr, and Ba (Fig. 6) and for Ca confirm that the major part of these elements was not introduced into the sediments by detrital minerals. However, characteristic units with specific slightly different features can be distinguished.

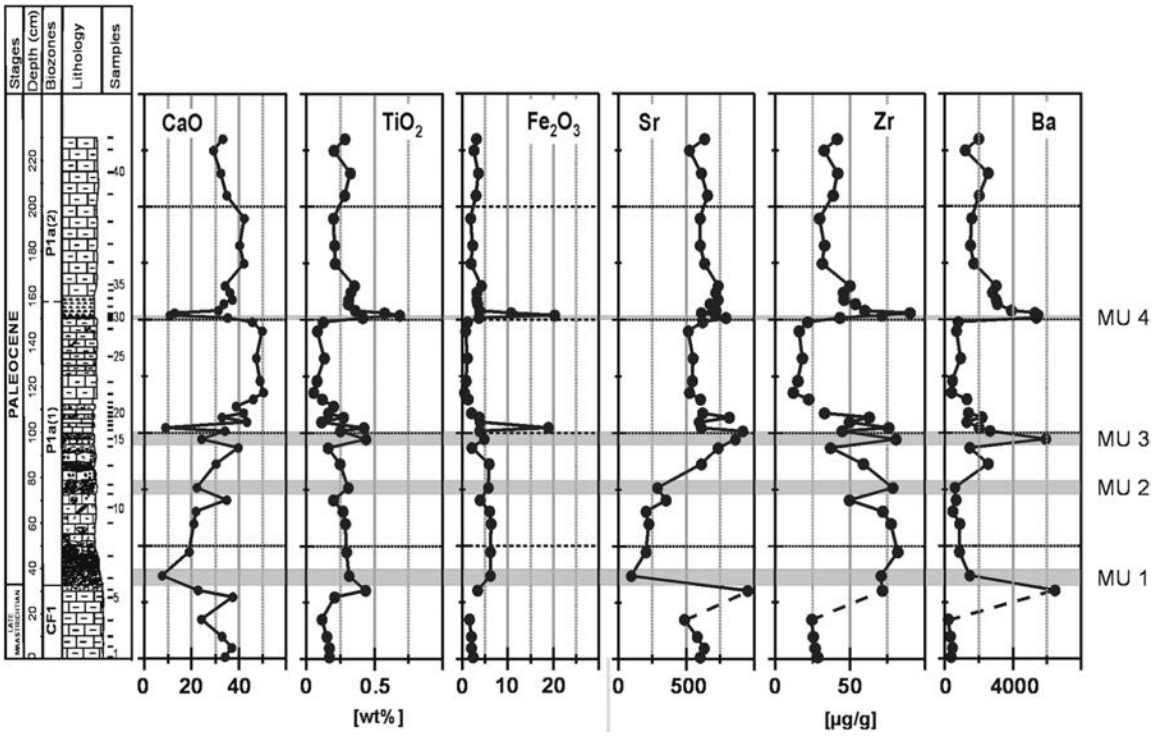

Figure 4. Distribution of CaO, TiO_2, Fe_2O_3, Sr, Zr, and Ba content along Cretaceous-Tertiary (K-T) section Beloc B3. (Lithology, stratigraphy, and biozones are redrawn from Stinnesbeck et al., 1999.)

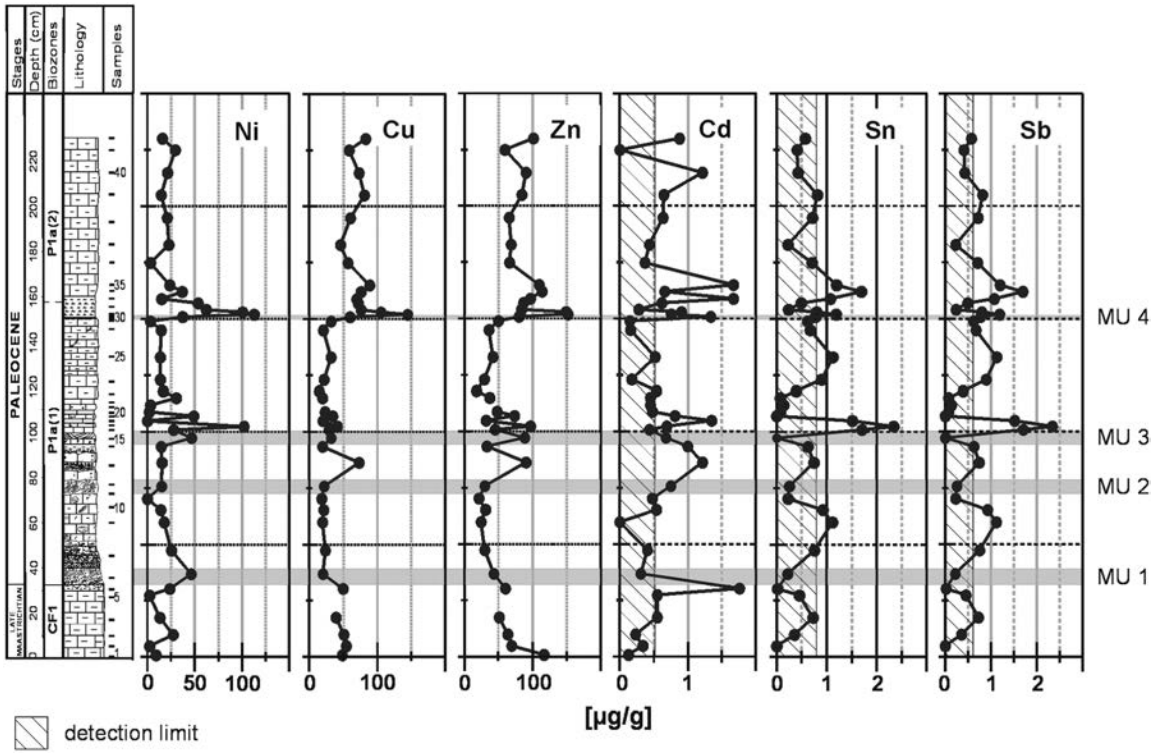

Figure 5. Distribution of Ni, Cu, Zn, Cd, Sn, and Sb content along K-T section Beloc B3. (Lithology, stratigraphy, and biozones are redrawn from Stinnesbeck et al., 1999.)

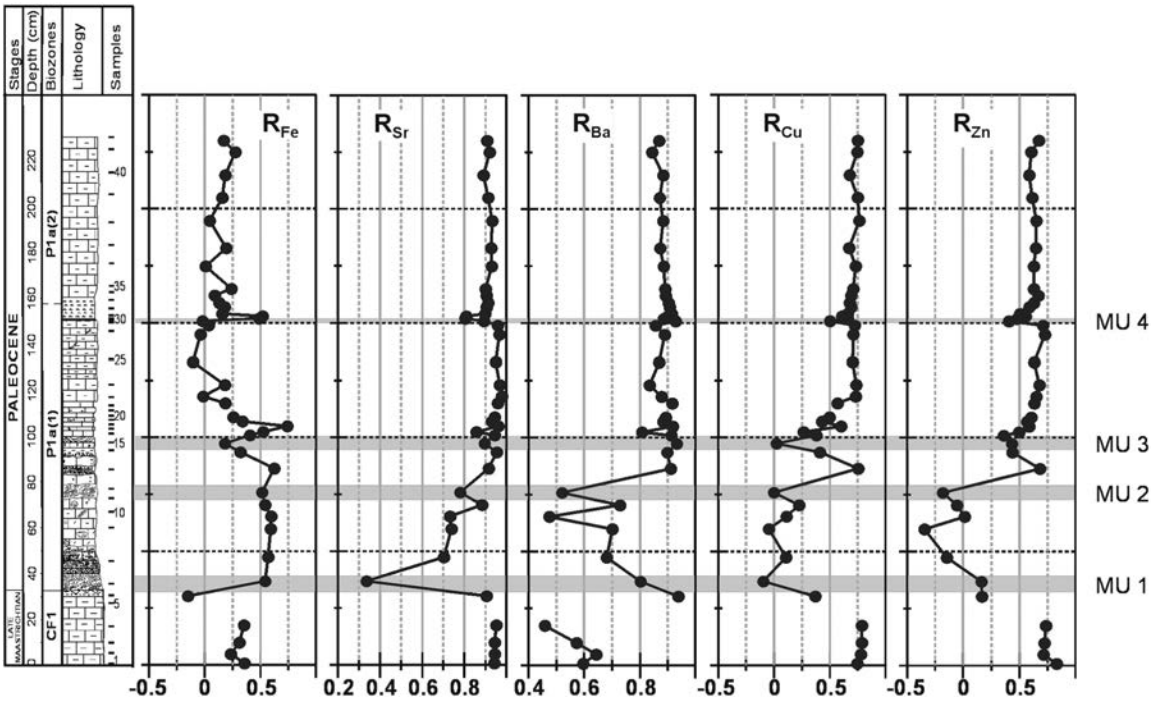

Figure 6. Excess ratios (R) of Fe, Sr, Ba, Cu, and Zn along Cretaceous-Tertiary (K-T) section Beloc B3. Excess ratios $R_{El} = El^*/El_{total}$ are estimates for ratio of part of element $El^* = El_{total} - [Ti_{sample}^* (El_{NASC}/Ti_{NASC})]$ not bound to detrital phase and bulk concentration El_{total}. R values can be interpreted as follows. $R \gtrsim 0.8$: only minor part of respective element is bound to detrital fraction of sediment; $R \sim 0.2$–0.8: significant part of element content is of detrital origin; $R \sim 0$: practically, entire amount of element is bound to detrital part of sediment; $R < 0$: detrital part of sediment derived from rocks with lower element/Ti ratios than North American Shale Composite (NASC) or Post-Archaean Average Australian Shale (PAAS) and/or part of respective element was lost during sedimentation or weathering. (Lithology, stratigraphy, and biozones are redrawn from Stinnesbeck et al., 1999.)

The Maastrichtian has a monotonous excess/bulk ratio, ~70% of the Fe and half of the Ba content being of terrigenous origin. Strontium, Cu, and Zn are controlled by incorporation in biogenic carbonates.

At the top of the Maastrichtian marly limestones (below the base of the spherule-rich deposit), increasing amounts of terrigenous and/or volcanic Fe, Cu, and Zn are indicated by the respective R values ($R_{Fe} = -0.2$; $R_{Cu} = 0.4$; $R_{Zn} = 0.2$; Fig. 6). The nondetrital fraction of Sr remains at high levels ($R_{Sr} \sim 0.8$) and that of Ba increases (R_{Ba} 0.4–0.95). A few centimeters above MU1 and to the top of the black spherule layer of MU2, Fe reaches maximum excess values ($R_{Fe} \sim 0.6$), except for the two Fe-rich horizons of MU3 and MU4. R_{Cu} and R_{Zn} fluctuate around 0. The nondetrital fraction of Sr shows a considerable drop in MU1 and increases upward to the top of MU2 ($R_{Sr} \sim 0.3$–0.8). Nonterrigenous Ba (Fig. 6) decreases in MU1 and shows considerable fluctuations to the top of MU2 ($R_{Ba} \sim 0.4$–0.7). Between MU1 and the top of MU2 reworking of different sediments is indicated by the high and variable contribution of the terrigenous and/or volcanic flux to the Cu, Zn, Sr, and Ba fractions together with a high and nearly constant excess rate of Fe.

At the base of both layers enriched in PGEs (MU3 and MU4) a slight increase in the fraction enriched in detrital components is observed for Cu, Zn, Sr, and Ba (Fig. 6).

In the limestone layers between MU3 and MU4, and in the marls above MU4, nearly all Fe can be assigned to the terrigenous and/or volcanic fraction with a small additional component increasing to the top of the profile. Copper, Zn, Sr, and Ba remain at nearly constant high excess rates, indicating accumulation of these elements by high biogenic carbonate sedimentation, by scavenging from the water column, and/or enriched authigenic minerals. The increase in detrital input as indicated by the R values of Sr, Ba, Cu, and Zn coincides with the influx of volcanic material.

To examine the possibility of a volcaniclastic input into the sediments the discrimination diagram proposed by Andreozzi et al. (1997) was used. Based on primary genetic differences in respect of the content and postdepositional behavior of some of the first-row transition elements (V, Ni, Cr) and immobile elements (Zr, TiO_2, Al_2O_3), Andreozzi et al. proposed a diagram in which volcaniclastic and normal terrigenous sediments define two separate areas and thus can be easily distinguished. Except for the two rust-colored, iron-rich layers (samples B3-17 and B3-29), all samples from the spherule-rich deposit (MU1, MU2, MU3, layers between) and from MU4 are much

closer to the field of the volcaniclastic deposits than are those from CF1, from Pla(1) above the spherule-rich deposit, and from Pla(2) (Fig. 7), suggesting that a volcaniclastic component was admixed to the entire spherule-rich deposit and MU4. However, it is not clear if remelting of crustal material by impact would confer a geochemical behavior (specifically higher mobility) to the transition metals, similar to that empirically observed in volcaniclastic deposits.

Platinum group elements

The concentrations of PGEs display variations of nearly two orders of magnitude (Table 3; Fig. 7). The lowest PGE concentrations, corresponding to background values for marine carbonates, are observed in the Maastrichtian part (basal 30 cm) of the section with 0.050 ng/g Ir, 0.2 ng/g Rh, <0.5 ng/g Pt, and 1 ng/g Pd. Above the K-T disconformity Ir increases slightly to 0.2 ng/g, whereas Pt, Rh, and Pd remain at low levels. In the rust-colored layer of MU3 (at 102 cm), Ir is enriched up to a factor of 20 compared to local Maastrichtian background values, whereas the other PGEs are only slightly enriched. Iridium concentrations tail below and above this marker unit (Fig. 7). In the limestones above MU3, Ir decreases to 0.2–0.3 ng/g, but is still slightly higher as compared to the Maastrichtian sediments. A second, Pt- and Pd-dominated, PGE anomaly is observed in the rust-colored layer and gray clay of MU4 (Fig. 7). Iridium is only enriched by a factor of 2 as compared with the marls below and above, whereas Pt is enriched to 6 ng/g and Pd to 9 ng/g. The chondrite-normalized PGE pattern of these samples is similar to that of ocean-floor basalts (e.g., Greenough and Fryer, 1990), Hawaiian basalts (Crocket and Kabir, 1988), or rift-related acid volcanics (Borg et al., 1987). The chondrite-normalized PGE pattern of the marly layers of normal pelagic sedimentation (17.5 and 195 cm, but also some of the samples belonging to MU2 and MU3) shows a distinct negative Pt anomaly. Because the residence time of Pt in the oceanic reservoir is much higher than for Pd (i.e., seawater is relatively enriched in Pt), a negative Pt anomaly is considered to reflect sedimentation in equilibrium with seawater (Tredoux et al., 1989).

Normalized to chondrite (McDonough and Sun, 1995) and plotted in order of decreasing melting points, the PGE pattern of MU3 is roughly chondritic (Fig. 9) and contrasts with the PGE pattern of the rest of the section. Chondritic PGE ratios are usually interpreted as indicating an extraterrestrial origin (Kyte et al., 1980; Ganapathy, 1980). The peak of the Ir anomaly is centered on a clayey layer strongly enriched in Fe-oxihydroxides. Because PGEs are readily scavenged by ferromanganese phases (at pH 7–9), their distribution in oxidized marine sediments is dominated by Fe-Mn oxihydroxide minerals (Anbar et al., 1996; Stüben et al., 1999), although other possibilities—such as precipitation with bacterial iron oxides, sulfides, and concentration from seawater into sediments—are considered (Wallace et al., 1990; Colodner et al., 1992). How-

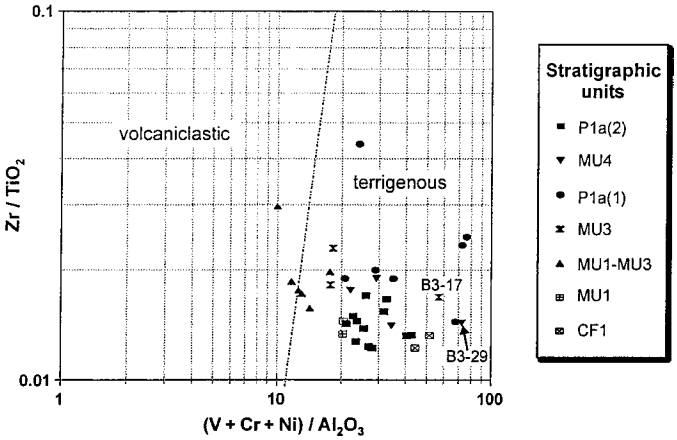

Figure 7. Discrimination diagram for sediments of volcaniclastic vs. terrigenous origin for different stratigraphic layers (according to Andreozzi et al., 1997). CF1 = *Plummerita hantkenoides* (CF1) zone of latest Maastrichtian; P1a(1) = lower *P. eugubina* (P1a[1]) zone of early Danian; P1a(2) = upper *P. eugubina* (P1a[2]) zone of early Danian.

TABLE 3. PLATINUM GROUP ELEMENT CONTENTS OF THE BULK SAMPLES

Sample #	Sampling depth (cm)	Ir (ng/g)	Pt (ng/g)	Rh (ng/g)	Pd (ng/g)
BE3-38	195	0.22	0.73	0.11	2.82
BE3-36	175	0.23	0.52	0.12	2.85
BE3-35	165	0.20	0.20	0.03	2.44
BE3-34	162	0.30	1.12	0.12	2.95
BE3-32	157	0.50	0.49	0.05	8.88
BE3-31	154	0.46	N.D.	N.D.	N.D.
BE3-30	153	0.29	0.78	0.02	7.54
BE3-29	152	0.56	6.19	0.11	8.10
BE3-28	151	0.14	0.11	0.00	2.92
BE3-26	145	0.19	N.D.	0.02	0.80
BE3-25	133	0.23	0.08	0.03	3.26
BE3-24	123	0.15	N.D.	0.02	1.15
BE3-22	115	0.27	4.93	0.05	2.42
BE3-19	107	0.59	N.D.	0.03	0.10
BE3-18	105	0.55	0.11	0.30	1.43
BE3-17	102.5	1.00	2.13	0.14	2.51
BE3-16	101	0.92	N.D.	0.05	N.D.
BE3-15	97.5	1.00	N.D.	0.09	0.06
BE3-14	93.5	0.66	0.39	0.04	2.04
BE3-12	76	0.28	0.19	0.09	0.63
BE3-10	65.5	0.26	N.D.	0.04	0.55
BE3-09	60	0.21	0.20	0.05	N.D.
BE3-08	47.5	0.20	N.D.	0.01	1.13
BE3-07	37	0.18	2.45	0.08	1.08
BE3-06	30.5	0.10	0.66	0.04	2.18
BE3-04	17.5	0.05	0.04	0.22	1.10
BE3-03	10	0.05	N.D.	0.40	1.40
BE3-01	1	0.09	0.61	0.18	1.82

Note: Platinum group element (PGE) contents of the bulk samples as determined by NiS fire assay and Inductively Coupled Plasma-Mass Spectrometry (ICP-MS). Neighboring samples were determined in different batches. The PGE contents display background values in the Maastrichtian, slightly elevated concentration in the Danian, and 2 PGE anomalies: an Ir-dominated one (samples Be3-14 to Be3-19) and a Pd-dominated one (samples Be3-29 to Be3-32).

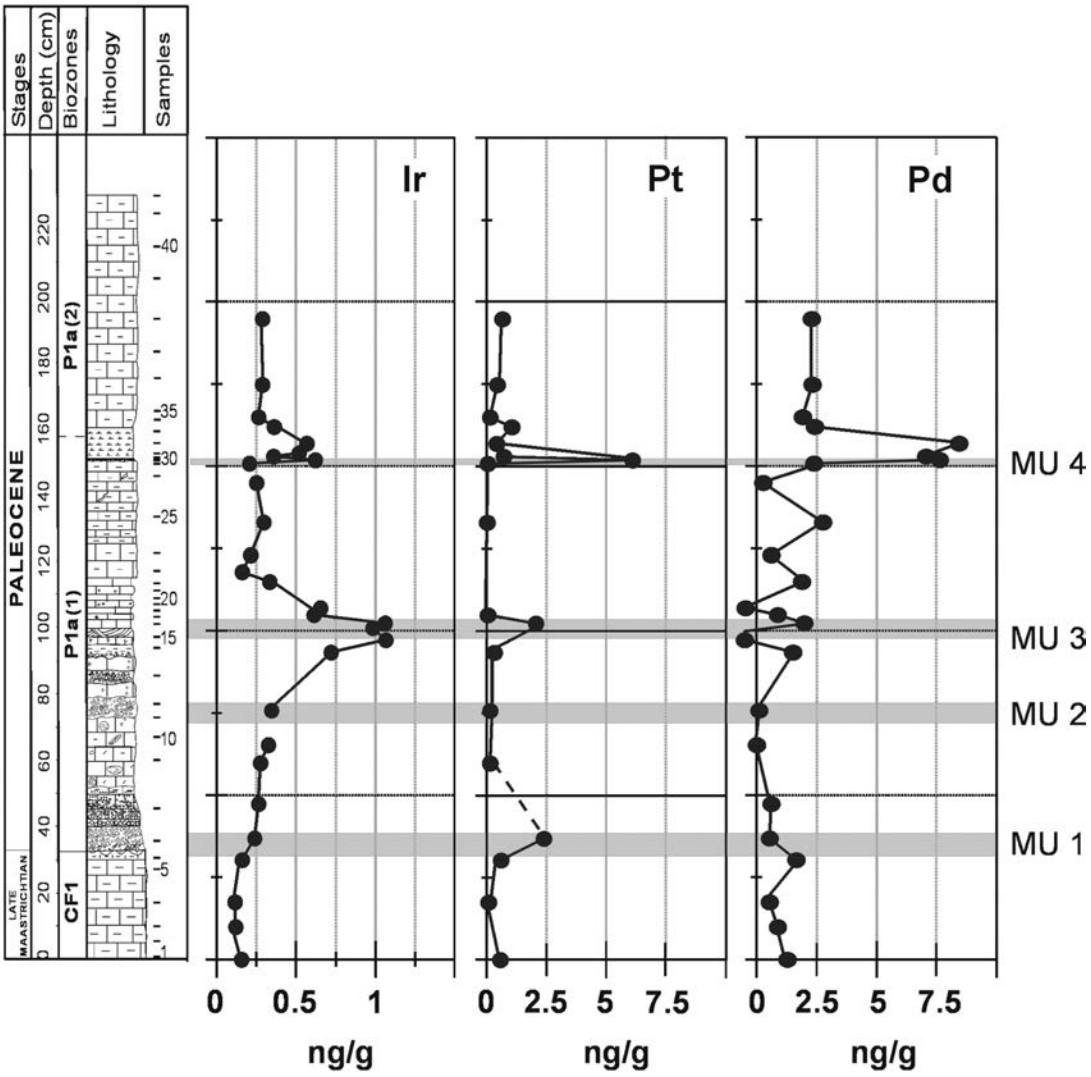

Figure 8. Ir, Pt, and Pd contents along Cretaceous-Tertiary (K-T) section Beloc B3 showing two different platinum group element anomalies for units MU3 and MU4 (Lithology, stratigraphy, and biozones are redrawn from Stinnesbeck et al., 1999.)

ever, unlike the PGE pattern of MU3, Fe-oxihydroxides and hydrogenous Mn crusts are enriched in Pt relative to the chondrite-normalized Pd contents (Stüben et al., 1999).

Below and above MU3, the anomalously high Ir contents show a gradual transition into the surrounding sediments over more than 50 cm (Fig. 8). Similar situations in several K-T sections have been mentioned (e.g., Crocket et al., 1988; Kyte et al., 1996; Rocchia et al., 1996; Rocchia and Robin, 1998; Smit, 1999), but the origin of such tailings is not clear. Considering possible primary depositional mechanisms resulting in such a profile, they would require prolonged periods of Ir input, if scenarios such as volcanic activity (Alvarez et al., 1980; Crocket et al., 1988) or a ring of projectile debris around the Earth following the impact of a huge extraterrestrial body (Rocchia and Robin, 1998) are envisaged. However, a number of other possibilities have been suggested to explain the gradual and sometimes symmetrical shape of the Ir anomalies, including erosion of ultramafic source rocks (Orth et al., 1988), gravitational or ballistic sorting of the ejecta during deposition (Evans et al., 1995), postdepositional redistribution during diagenesis or weathering (Wallace et al., 1990; Colodner et al., 1992), microbial activity (Dyer et al., 1989), carbonate dissolution (Rocchia et al., 1990), and physical mixing by bioturbation (Evans et al., 1995; Smit, 1999).

The diffuse extension of the Ir concentrations above the MU3 is probably mainly a consequence of the long residence time of the Ir in the oceanic reservoir (to 20 k.y.; Anbar et al., 1996) as a result of a meteorite impact, as suggested by Rocchia and Robin (1998). However, a different explanation is necessary to explain the tailing of the Ir values into the underlying

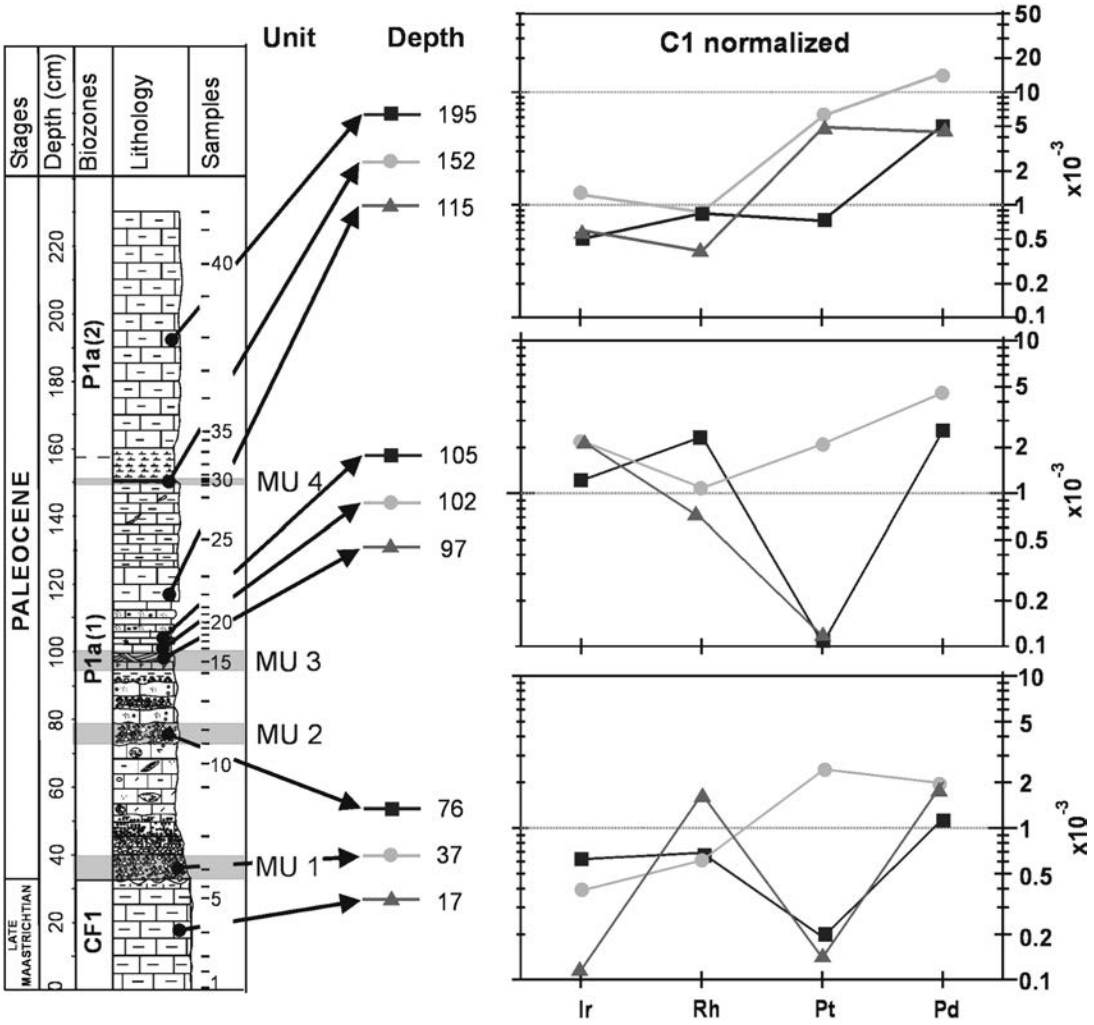

Figure 9. Chondrite-normalized platinum group element (PGE) patterns of defined sediment horizons: Maastrichtian marls (17 cm) of lower section, marker units MU1 (37 cm), MU2 (76 cm), MU3 (97 cm, 102.5 cm; Ir anomaly), MU4 (152 cm; upper PGE anomaly), and Paleocene marls of upper section (105 cm, 115 cm, and 195 cm). Normalization C1 values are from McDonough and Sun (1995).

sediments. Despite their known low mobility, several observations seem to support the possibility of a postdepositional chemical redistribution of the PGEs, as a consequence of redox changes in the sediments (Wallace et al., 1990; Colodner et al., 1992; Anbar et al., 1996). The behavior of the individual elements is slightly different in this respect, but the conclusions are equivocal and only little experimental work was carried out to substantiate these observations (Dai et al., 2000). For example, while some (Colodner et al., 1992; Evans et al., 1994; Anbar et al., 1996) relate the remobilization of Ir to reduction of oxic sediments driven by degradation of organic matter, others (e.g., Bowles, 1986; Wallace et al., 1990; Sawlowicz, 1993) consider that PGEs are carried as chloride or organic complexes by highly oxidized acidic fluids and are redeposited when they interact with low-Eh brines. A postdepositional remobilization of the PGEs cannot be undoubtedly demonstrated in the section examined.

Palladium shows the highest chondrite normalized values compared to other PGEs ($>1 \times 10^{-3}$), except for the reworked horizon at 37 cm. For example, in sample B3-17 (MU3, red layer at 102.5 cm), the chondrite-normalized values for Ir and Pt are much lower ($\sim 2 \times 10^{-3}$ for Ir and Pt) than for Pd ($\sim 5 \times 10^{-3}$) (Fig. 9), indicating that the material was depleted more in Ir and Pt than in Pd (accepting an extraterrestrial source). Such a fractionation pattern (presuming that it is due to postdepositional mobilization) would not be in agreement with the general mobility of the PGEs during diagenesis and weathering, which generally appears to decrease approximately in order Pd $\gg$ Pt $>$ Rh $>$ Ru $>$ Os $>$ Ir (Westland, 1981). Regardless of the mechanisms considered, the postdepositional

mobilization of PGEs should be accompanied by the redistribution of many transition metals (Wallace et al., 1990; Colodner et al., 1992). Such redistribution cannot be unambiguously proved in the Beloc 3 section. In both MU3 and MU4, the highest Ir contents are related to thin Fe-rich layers. Elements such as As and Sb, which are typically bound to Fe-oxihydroxides and are readily removed if a redox front moves through the sediment, show very sharp maximums in the Fe-rich layers, without any signs of mobilization. Nevertheless, covariation of the Ir content with some of the heavy metals (e.g., Cu, Zn, Pb) across the MU3 horizon can be demonstrated. However, this seems more likely to be a primary feature controlled by the mineral composition, because the higher metal contents coincide with the presence of spherules and correlate with the amount of their alteration products (smectites, zeolites). We think that, rather than postdepositional remobilization, the tailing of the Ir content below MU3 is related to sediment reworking, as a result of a high-energy depositional environment, as indicated by biostratigraphic, sedimentologic, and granulometric data (Stinnesbeck et al., 1999; Keller et al., 2001). Nevertheless, a postdepositional mobilization of the PGEs cannot be completely excluded.

The slight deviation of the Ir anomaly from a typical chondritic pattern suggests that other influxes, such as volcanic emission or some other magmatic input, may also have been contributing factors. Dunites associated with a dismembered ophiolite suite of Upper Cretaceous age on Jamaica, and a suite of ultramafic rocks forming the lower part of a plutonic complex of island arc affinity of mid-Cretaceous age on Tobago, can be considered possible sources for PGEs in the Caribbean area. From both localities, Ni-Cu mineral assemblages enriched in PGEs associated with a primary stage of metallization, and individual PGE mineral phases were reported (PtS, grains composed of Rh, Ir, Pt, Cu, As, and S, native copper enriched in Pt and Pd, to 23 wt% and 15 wt%, respectively) (Scott et al., 1999).

Rare earth elements

The most important factor controlling the REE content of terrigenous sediments is the mineralogical composition and the provenance (McLennan, 1989; Condie, 1991). The REEs are chiefly transported with particulate matter or adsorbed phases. Because they are not easily fractionated during transport, sedimentation, diagenesis, and weathering, they generally reflect the chemistry of their source. Argillaceous rocks therefore frequently display a pattern that is very close to the average of the upper continental crust, being enriched in the light REEs and presenting an almost ubiquitous negative Eu anomaly (McLennan, 1989). Deviations from the crustal average are primarily due to specific mineralogical composition. Among these, heavy minerals (e.g., apatite, monazite, allanite, zircon) can easily dominate the REE pattern of sedimentary rocks because of their high concentrations in REEs (e.g., McLennan, 1989; Ohr et al., 1994). Plagioclase preferentially concentrates divalent Eu during igneous processes, and sedimentary rocks enriched in plagioclase (e.g., volcanogenic graywackes) will inherit this pattern. Low to moderate contents of amphiboles generally do not alter substantially the average pattern of the sedimentary rocks. Quartz and carbonate, due to their very low REE contents, have mostly a dilution effect, generally lowering the REE contents well below that of average shales. In foraminiferal tests, the slight enrichment of the middle REEs leads to a roof-shaped pattern (Palmer, 1985; Winter et al., 1997). Marls with a higher proportion of biogenic carbonate will have relatively low chondrite-normalized La/Sm and Gd/Yb ratios. Seawater is characterized by a distinct negative Ce anomaly, and authigenic phases formed in equilibrium with seawater will inherit this feature (Fleet, 1984). Distribution patterns similar to seawater have been reported in limestones and calcareous oozes (Taylor and McLennan, 1985; Pattan et al., 1995; Sethi et al., 1998). Because of the low mobility of the REEs, diagenetic alteration and weathering of the detrital, biogenic, and authigenic components will not affect substantially the original distribution of the lanthanides in the sediment. However, stronger remobilization may occur during the alteration of glass fragments, spherules, and volcanogenic minerals (e.g., Elliot, 1993).

In the bulk samples investigated, REE contents are 5–15 times the chondritic values, with moderate enrichments of the light over the middle REEs ($La_{Ch\text{-}N}/Sm_{Ch\text{-}N}$ = 1.9–3.8) and flat heavy REE patterns ($Gd_{Ch\text{-}N}/Yb_{Ch\text{-}N}$ = 0.9–1.3) (Table 4; Fig. 10). Compared with the NASC, the total REE contents are ~4 times lower (excepting the more depleted sample from MU1) and the samples are slightly depleted in the light lanthanides relative to the heavy lanthanides (La_{NASC}/Yb_{NASC} = 0.4–0.7). The generally low REE contents relative to NASC are due to variable amount of carbonate admixed, while the depletion of the relatively more mobile light REEs could be connected to a slight remobilization during late diagenesis (Hannigan and Basu, 1998).

The chondrite-normalized REE patterns observed throughout the section can be conveniently subdivided into three groups, types 1–3.

Type 1 displays negative Ce and Eu anomalies (Ce/Ce* = 0.58 and Eu/Eu* = 0.81, respectively) and is typical for the Maastrichtian marly limestones. The pattern can be explained by the mixing of detrital clay with carbonate material. The clay fraction confers to the samples a typical crustal pattern with a negative chondritic Eu anomaly, while the carbonate lowers the REE contents of the bulk samples and imprints a negative Ce anomaly (Pattan et al., 1995).

Type 2 is characterized by the absence of a Ce anomaly and is encountered in the samples of the spherule-rich deposit (including the base of MU3, at 97.5 cm). This feature is not restricted to the spherule-rich layers of the spherule-rich deposit (MU1 and MU2), but is also found in the interlayered marls (at 65 and 86 cm). The chondrite-normalized Eu anomalies show

TABLE 4. RARE EARTH ELEMENT CONTENTS IN BULK SAMPLES AND SPHERULES

Sample number	Sampling depth (cm)	Sc (µg/g)	Y (µg/g)	La (µg/g)	Ce (µg/g)	Pr (µg/g)	Nd (µg/g)	Sm (µg/g)	Eu (µg/g)	Gd (µg/g)	Tb (µg/g)	Dy (µg/g)	Ho (µg/g)	Er (µg/g)	Tm (µg/g)	Yb (µg/g)	Lu (µg/g)
Bulk samples																	
B3-32	157.0	12.6	14.4	10.1	10.4	1.93	8.52	1.87	0.81	2.35	0.37	2.43	0.53	1.62	0.24	1.58	0.23
B3-29	152.0	15.4	8.5	5.1	8.5	1.32	6.18	1.54	1.03	1.87	0.27	1.79	0.37	1.13	0.17	1.25	0.18
B3-28	151.0	11.5	15.2	10.0	10.8	1.96	8.65	1.90	1.26	2.38	0.37	2.38	0.52	1.59	0.25	1.57	0.22
B3-16	101.0	9.0	10.4	8.7	11.9	1.78	7.51	1.65	0.74	1.94	0.29	1.89	0.39	1.23	0.19	1.27	0.18
B3-15	97.5	16.4	4.8	4.4	7.9	1.07	4.35	0.99	0.10	1.06	0.17	1.11	0.23	0.74	0.12	0.93	0.14
B3-13	86.5	10.1	6.4	5.0	10.9	1.48	6.25	1.49	0.13	1.56	0.25	1.57	0.31	0.95	0.16	1.08	0.16
B3-12	76.0	14.1	7.5	8.2	19.4	2.19	8.91	1.97	0.51	1.98	0.30	1.91	0.37	1.14	0.18	1.27	0.19
B3-10	65.5	12.5	5.0	5.5	12.7	1.62	6.65	1.56	0.37	1.50	0.24	1.52	0.29	0.88	0.16	1.24	0.19
B3-07	37.0	15.9	2.5	2.2	5.1	0.69	2.99	0.71	0.30	0.70	0.11	0.63	0.12	0.37	0.07	0.47	0.08
B3-03	10.0	8.0	17.1	12.0	12.4	2.24	9.73	2.01	0.61	2.61	0.41	2.74	0.58	1.81	0.28	1.64	0.25
Spherules																	
B3-12	Dark	21.4	26.8	21.2	46.0	5.37	23.3	4.80	1.35	4.70	0.68	4.42	0.92	2.77	0.43	2.86	0.42
B3-12	Yellow	21.4	26.4	21.2	45.6	5.17	22.6	4.73	1.23	4.29	0.71	4.34	0.83	2.59	0.36	2.77	0.38
B3-12	Smectite	12.4	1.2	0.9	2.0	0.27	1.20	0.27	0.17	0.24	0.04	0.23	0.05	0.13	0.02	0.14	0.02

Note: Rare earth element contents in bulk samples and spherules, determined by inductively coupled plasma-mass spectrometry (ICP-MS). The rare earth element (REE) contents of the bulk samples indicate depositional changes and fluctuation in the source and nature of the deposited materials. The REE contents of glass spherules are 20 times higher than those of smectite spherules.

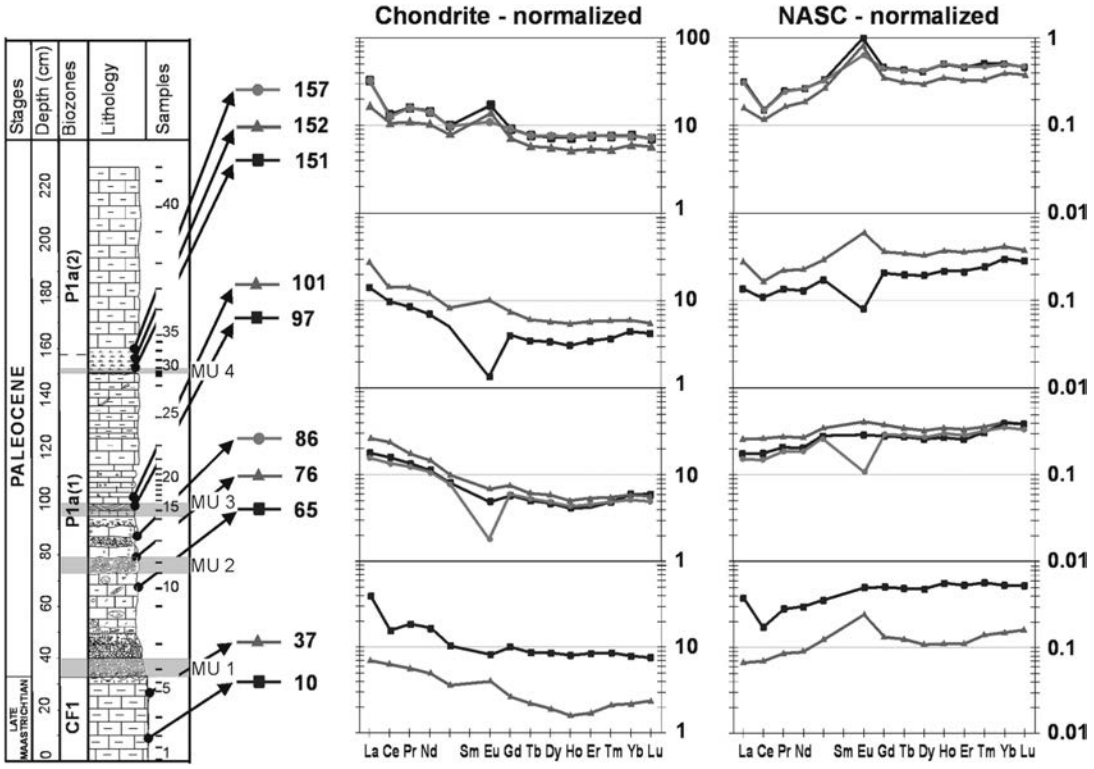

Figure 10. Chondrite-normalized and North American Shale Composite (NASC) normalized rare earth element (REE) patterns of distinct sediment layers of different horizons of Cretaceous-Tertiary (K-T) section, Beloc. Normalization values are from McDonough and Sun (1995, chondrites) and Gromet et al. (1984, NASC).

an apparently systematic change upsection, with slightly positive values at MU1 (Eu/Eu* = 1.31), and progressively lower values upsection (from Eu/Eu* = 0.73–0.80 to 0.30 in MU3). The absence of a Ce anomaly in the spherule-rich deposit, in contrast to the sequences below and above, could indicate that these sediments were not formed in equilibrium with seawater, but were deposited faster. However, a change in the redox state of the seawater may be an alternative explanation for the lack of Ce anomalies (see following). The formation of secondary mineral phases (smectites and/or palagonite, zeolites, opal)

from glass has certainly affected the original distribution of the REEs in the spherule-rich deposit to some extent. However, a direct relationship between the composition of the smectitic spherules and that of the known glass varieties could not be demonstrated (see following). However, it is noteworthy that the REE pattern of the bulk samples B3-7 (MU1, with a slight chondritic negative Eu anomaly) and B3-12 (MU2) can be closely modeled by the mixing of glass and smectite with a composition similar to that of the spherules analyzed from sample B3-12 in a proportion of 10% to 90% and 35% to 65%, respectively (Fig. 11). (Because of the relatively low CaO contents of these samples and the low concentrations of REEs in calcite, the influence of carbonate was disregarded.) The modeling is based on mass-balance acceptances, and was solved by successive iterations until the best fit was obtained. Guy et al. (1999) reported that REE concentrations in clays resulting from seawater-basalt interaction are close to that of unaltered basalt, while concentrations in zeolites are 10 times lower. However, the fate of REEs during the alteration of volcanic ash and glass material to smectite and zeolite (regardless of the origin of glass) is not well understood. Available data are not sufficient or conclusive (Hopf, 1993; Martin-Barajas and Lallier-Verges, 1993; Terakado and Nakajima, 1995; Christidis, 1998) and preclude further interpretation of our REE data with respect to glass alteration.

Type 3 is restricted to the gray-green shale of MU3 (101 cm) and to the samples around MU4. Compared to type 1, type 3 is characterized by a positive Eu anomaly (Eu/Eu* = 1.18–1.85) in addition to the negative Ce anomaly (Ce/Ce* = 0.53–0.79). The Eu anomaly is considerably higher in MU4 (Eu/Eu* = 1.81–1.85), where it may be related to higher feldspar contents or to its alteration products. However, in the absence of mineralogical proof the development of a positive Eu anomaly may be interpreted as a result of diagenetic reprecipitation, promoted by compaction and reduced pore waters enriched in Eu^{2+} entering an oxidizing environment (MacRae et al., 1992). This mechanism is supported by the presence of the oxidized, Fe-rich layers at or in close proximity to the samples with the highest Eu anomalies. The REE pattern of the gray-green clay of MU3 (at 101 cm) is almost identical to that of the samples from MU4. Except for the positive Eu anomaly, the total REE content and the presence of a characteristic negative Ce anomaly are similar to that found in the clay fraction of the Fish Clay horizon of the K-T transition at Stevns Klint, Denmark (Tredoux et al., 1989; Elliot, 1993). The negative Ce anomaly was interpreted by Elliott (1993) to be the result of possible equilibration with seawater; the Mg-smectites he investigated were formed authigenically from a volcanic glass precursor.

Several authors reported systematic stratigraphic trends in the distribution of Ce anomalies. Such trends were interpreted to reflect changes in the oceanic redox conditions (e.g., Hu et al., 1988; Shields and Stille, 1998) or in the tectonic depositional environment (Murray et al., 1990). According to Shields and Stille (1998), the correlation of the Ce anomaly with other proxy parameters (Sr and Nd isotope ratios, $\delta^{13}C$ of carbonate and organic fraction, primary sedimentological features) proves that the Ce anomaly reflects primary changes in the redox state of coeval seawater. On the basis of the good correlation between the Ce anomaly and $\delta^{13}C$ of carbonate ($r = -0.86$) and assuming that no suboxic or anoxic diagenesis has taken place, we conclude that the seawater was less oxygenated during the sedimentation of the spherule-rich deposit as compared to the sequences below and above.

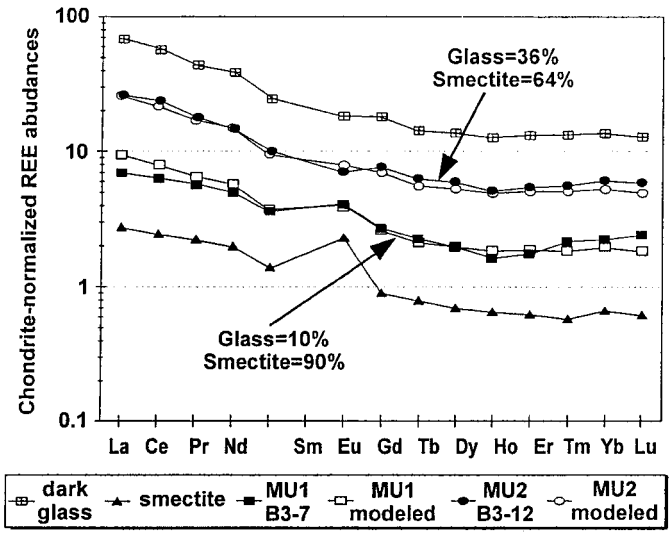

Figure 11. Simulated rare earth element (REE) pattern of bulk samples from MU1 (B3-07) and MU2 (B3-12) by mixing glass and smectite spherules with compositions similar to those analyzed from sample B3-12.

Stable isotopes

During diagenesis, primary biogenic carbonate can be dissolved and replaced by secondary calcite with a different isotopic composition. Oxygen isotopic values of bulk carbonate are more sensitive to postdepositional alteration than carbon isotopic ratios. An increase in temperature caused by sediment burial and possibly different isotopic composition of pore fluids are the most important factors altering the primary isotopic signal of biogenic calcite (Killingley, 1983; Jenkyns et al., 1994; Schrag et al., 1995; Mitchell et al., 1997). Generally, both of these factors tend to lower the initial oxygen isotopic values. Consequently, if a part of the carbonate was affected by recrystallization, the excursions toward more negative $\delta^{18}O$ values may represent diagenetically altered isotopic values, whereas higher values should be regarded as minimum values.

Bulk $\delta^{13}C$ values range between 0.37‰ and 0.65‰ in the latest Maastrichtian marly limestones and decline to −3.34‰ at the base of MU1 with a further decline to −4.85‰ above MU1 (Table 2; Fig. 12). This negative $\delta^{13}C$ shift in the early Danian P1a(1) sediments reflects the drop in primary produc-

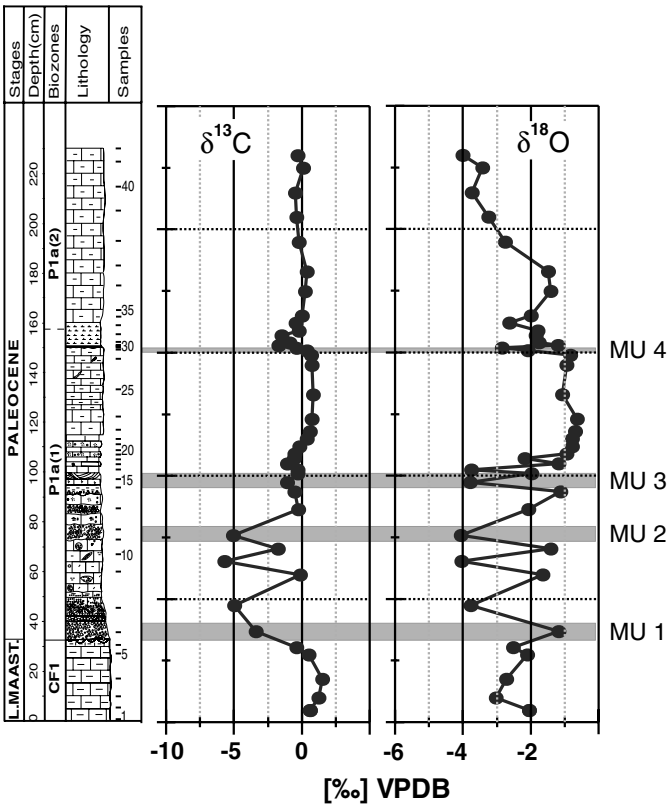

Figure 12. Carbon and oxygen isotope data of carbonate fraction in section Beloc B3 with oscillating pattern for both isotopes within spherule-rich deposit, negative $\delta^{13}C$ shift in early Danian, and with values stabilized at −1.0‰ $\delta^{18}O$ between MU3 and MU4 and gradual decrease to −4.0‰ near top of section. VPDB is Vienna Peedee belemnite. (Lithology, stratigraphy, and biozones are redrawn from Stinnesbeck et al., 1999.)

tivity across the K-T boundary, though the shift at Beloc is larger (3.3–4.9) than in other tropical marine sequences (~2‰–3‰) (Keller and Lindinger, 1989; Zachos et al., 1985, 1989). Between MU1 and 2, $\delta^{13}C$ values oscillate (−0.09‰ to −5.65‰) and may reflect mechanical reworking of Cretaceous sediments into Danian deposits. The original signal also may have been overprinted by diagenetic effects from the sparry calcite matrix that cements the spherule debris. In the limestone between MU2 and MU3, $\delta^{13}C$ values vary between 0‰ and −1.0‰ with a 0.5‰ excursion associated with the Ir-dominated PGE anomaly. In the limestone above MU3, $\delta^{13}C$ values increase from −1.0‰ to +0.5‰ and remain stable to MU4, when they drop by more than 2‰ (Fig. 12). Consequently, $\delta^{13}C$ values narrowly fluctuate around 0‰. The two negative excursions associated with the PGE anomalies may reflect short-term changes in primary productivity, although because they coincide with very low to nearly absent calcite, they may be artifacts of the sedimentary record.

Oxygen isotope values range between −4.05‰ and −0.77‰; Maastrichtian values vary between −2.0‰ and −3.0‰ (Table 2). Between MU1 and MU3 (spherule-rich deposit and bioclastic limestone,Fig. 12), $\delta^{18}O$ values oscillate between −4.0‰ and −2.0‰, probably due to the presence of Cretaceous reworked sediments and diagenetic alteration. In the pelagic limestone, between MU3 and MU4, values stabilize between −0.5‰ and −1.0‰ and gradually decrease to −4.0‰ near the top of the section. Diagenetic alteration of the carbonate as well as reworked sediments in the lower part of the section (zone P1a[1]) impede the use of the $\delta^{18}O$ bulk record as a temperature record, but some trends in the *Parvularugoglobigerina eugubina* zone are apparent. For example, temperature appears to have been relatively cool between MU3 and MU4 (upper P1a, lower *P. eugubina* zone) and gradually warmed above MU4 (P1a[2], upper *P. eugubina* zone). Temperature trends between MU1 and MU3 are obscured by abundant reworked sediments, but suggest overall cool climates (Fig. 12).

Chemical, mineralogical, and isotopic correlations

The hierarchical clusters deduced from the Spearman rank correlation matrix (Fig. 13) of minerals, stable isotopes, and major and trace elements display a clear grouping that reflects the mineralogy and chemistry of the parent material and chemical mobility of the elements. One group, consisting of $CaCO_3$, CaO, MnO, and loss on ignition (LOI), corresponds to marine biogenic or chemical carbonate precipitation. The second group combines minerals and elements of mainly terrigenous, detrital, and/or volcanic origin (SiO_2, TiO_2, Al_2O_3, Fe_2O_3, MgO, Na_2O, Zr, Nb, phyllosilicates, and Ga). Barium is closely correlated with zeolites and to a lesser extent with Sr and weakly with Ir. The close correlation of zeolites and Ba may be caused by the release of Ba and Sr from chemical weathering of feldspars followed by adsorption on clay and Fe oxides and coprecipitation into the sediment. Thus variations in biogenic carbonate deposition are overprinted by this effect, and should be used with caution as paleo-sea-level proxies (Stoll and Schrag, 1996, 1998). The association of Pd with Br, which is probably scavenged from seawater, may be an indication of higher solubility of Pd in seawater compared to the other PGEs in the profile (Sawlowicz, 1993; Stüben et al., 1999). The weak association of Pt and Ni is a reflection of the enrichment of Pt and Ni in the gray clays and the upper rust-colored layer of MU4.

Spherules

Three types of spherules (dark glass, yellow glass, and smectite spherules) were separated from the spherule-rich deposit in MU2 (sample B3-12) and analyzed by electron microprobe for major elements and by ICP-MS for REEs. The major element chemistry indicates two different types of glassy spherules and a significant chemical difference between the glass and smectite spherules (Tables 4 and 5).

The black glass is relatively homogeneous, with an andesitic to dacitic composition, similar to that found by Izett (1991),

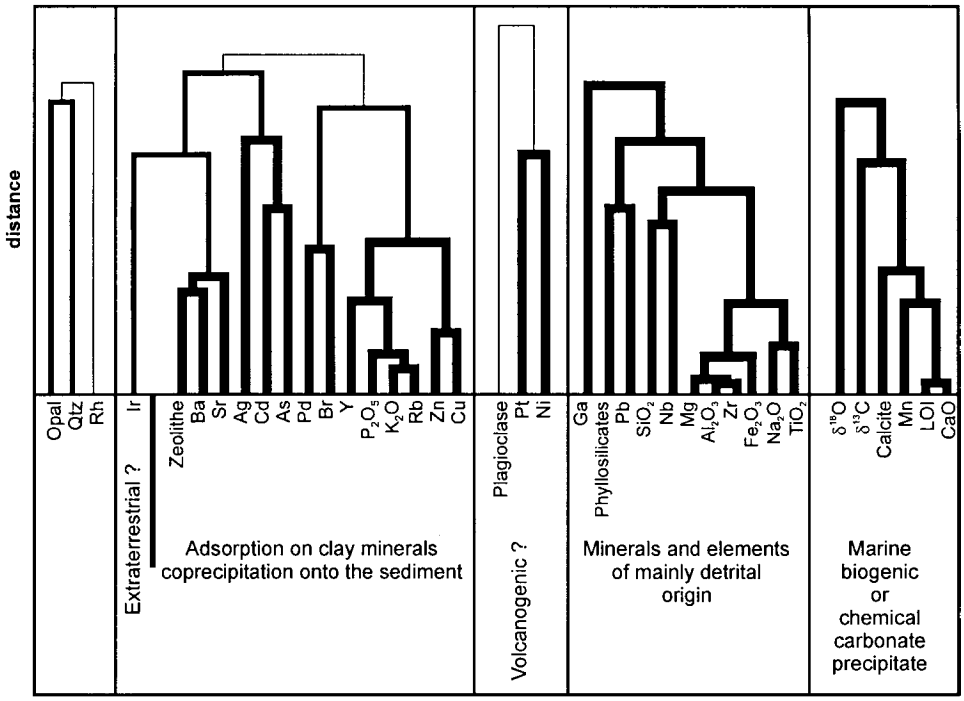

Figure 13. Hierarchical cluster analyses of Spearman rank correlation matrix (Rock, 1988) of minerals, stable isotopes, and major and trace elements from Beloc B3 showing five different groups. LOI is loss on ignition.

TABLE 5. MAJOR ELEMENT COMPOSITION OF SPHERULES FROM SAMPLE B3-12 (MICROPROBE DATA)

		FeO (wt%)	MnO (wt%)	SiO_2 (wt%)	MgO (wt%)	K_2O (wt%)	CaO (wt%)	TiO_2 (wt%)	Na_2O (wt%)	Al_2O_3 (wt%)	Total (wt%)
4 black glass spherules (18 points)	avg.	5.31	0.15	66.85	2.75	1.53	5.38	0.65	1.96	14.94	99.52
	stdv.	0.36	0.05	1.28	0.20	0.11	0.54	0.05	0.37	0.29	
	min.	4.79	0.06	64.61	2.39	1.33	4.79	0.54	1.51	14.48	
	max.	5.92	0.22	68.94	3.11	1.75	6.58	0.74	2.63	15.47	
	Q1	4.99	0.12	66.12	2.65	1.45	5.06	0.63	1.68	14.77	
	Q3	5.52	0.19	67.51	2.91	1.61	5.44	0.68	2.32	15.06	
2 yellow glass spherules (8 points)	avg.	5.37	0.15	60.47	3.16	1.40	11.45	0.65	2.78	14.21	99.63
	stdv.	0.60	0.07	4.49	0.55	0.42	5.29	0.06	0.30	0.82	
	min.	4.59	0.06	51.07	2.60	0.63	8.24	0.55	2.13	12.65	
	max.	6.22	0.27	64.33	4.35	1.98	23.13	0.73	3.11	15.19	
	Q1	4.95	0.11	59.60	2.80	1.30	8.30	0.61	2.72	13.81	
	Q3	5.78	0.18	63.92	3.31	1.66	11.37	0.69	2.95	14.79	
Coating of 3 smectitic spherules (10 points)	avg.	5.07	0.01	61.98	3.92	1.13	1.06	0.81	0.05	9.82	83.84
	stdv.	1.81	0.01	4.41	1.42	0.49	0.29	0.13	0.02	3.25	
	min.	0.63	0.00	53.79	0.02	0.24	0.64	0.64	0.01	0.76	
	max.	7.73	0.02	68.13	4.92	1.89	1.49	1.11	0.08	11.75	
	Q1	4.75	0.00	60.65	4.01	0.93	0.80	0.73	0.03	10.08	
	Q3	5.84	0.01	65.50	4.68	1.41	1.25	0.84	0.06	11.39	
3 smectitic spherules (9 points)	avg.	4.81	0.01	65.26	4.64	1.10	0.88	0.34	0.06	11.12	88.23
	stdv.	0.41	0.02	3.21	0.40	0.43	0.16	0.13	0.02	0.83	
	min.	4.31	0.00	59.61	3.95	0.15	0.67	0.15	0.03	9.83	
	max.	5.32	0.06	69.58	5.19	1.56	1.16	0.49	0.08	11.98	
	Q1	4.41	0.00	63.25	4.45	0.99	0.78	0.30	0.04	10.66	
	Q3	5.15	0.01	67.82	4.93	1.29	0.93	0.45	0.07	11.82	

Note: Glass, Ca-rich and Ca-poor, and two types of smectites, rims as weathering products of glass spherules, which are slightly enriched in TiO_2 compared to the glass, and spherules depleted in TiO_2 compared to the glass.
avg. = average, stdv. = standard deviation, min. = minimum, max. = maximum, Q1 = first quartile, Q3 = third quartile.

Koeberl and Sigurdsson (1992), Koeberl (1993). Sulfur was not detected in the black glass fragments. The yellow glass is largely zoned, showing flow structures with varying CaO contents (the CaO content varies between 8 and 23 wt% along these structures) within one single grain with a significant spatial correlation of Ca and S (Fig. 14A). Sulfur content, $\delta^{34}S$ values, and B isotopes of yellow glass fragments are thought to result from inclusion of evaporitic material (Chaussidon et al., 1996), although Koeberl (1993) showed that B isotopes are incompatible with an evaporitic source and trace elements are not in agreement with any combination of materials from Chicxulub analyzed by him at that time. Based on oxygen isotope data, Blum and Chamberlain (1992) also rejected the involvement of a sulfate-rich evaporitic material, and argued for the mixture of carbonate and silicate rocks. The oxygen, Sr, and Nd isotopic composition of the Haitian glass spherules proved to be practically identical with those of Chicxulub melt rocks (Blum et al., 1993). Recalculating the uncontaminated composition of the glass by removing the excess CaO, a source rock of dacitic composition similar to the black glass results.

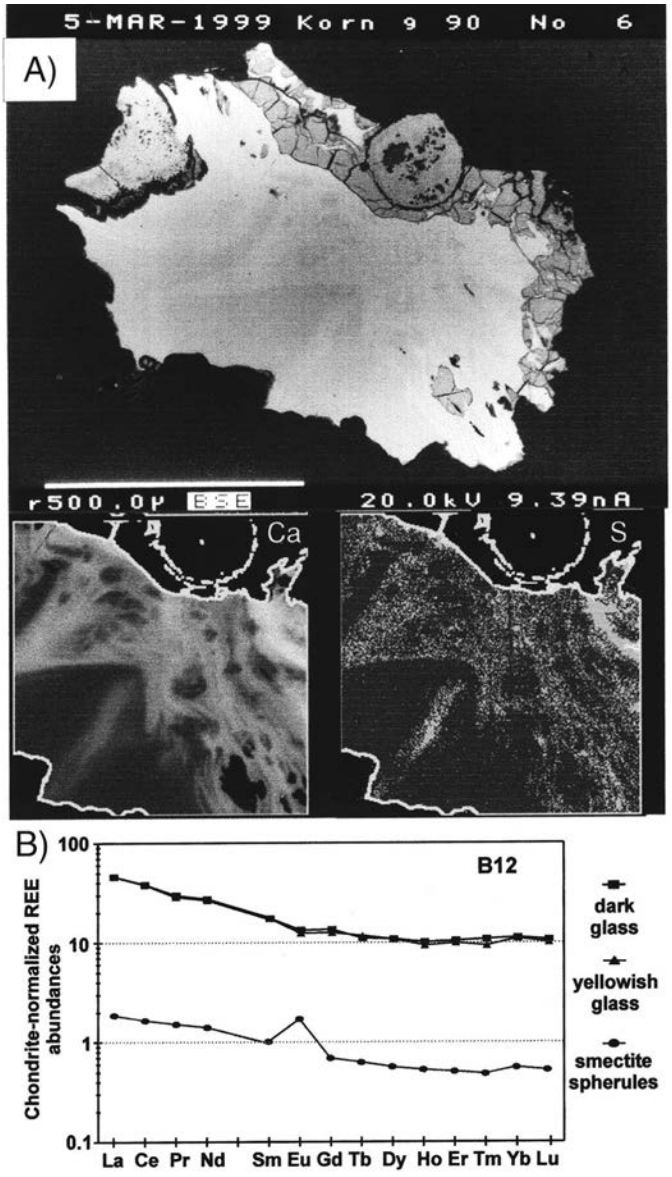

Figure 14. A: Microphotographs of Ca-rich glass spherule (sample B3-12) from spherule-rich deposit at Beloc B3, showing backscatter electron image and distribution of Ca and S within spherule. Yellow glass is largely zoned, showing flow structures with varying CaO contents. B: Chondrite-normalized rare earth element (REE) patterns of two glass spherules and one smectite spherule from spherule-rich deposit at Beloc B3 (sample B3-12).

For the degassing experiments two spherule samples were taken from B3-7 (MU1) and B3-12 (MU2). The interpretation of the evolved gas analyses (EGA curves) is based on the partial pressure curves of the evolved gas species. Only the gas-release curve above 1000°C is due to degassing of the melt and is considered to carry a primary signal. The spherule (B3-12) in MU2 is slightly altered, as demonstrated by water release already well below 1000°C, which can be assigned to the degradation of some alteration products. Distinct spikes in the partial pressure curve well above 1000°C correspond to SO_2, which supports the uptake of SO_2 from evaporites into the silicate melt, as argued by Chaussidon et al. (1996) on the basis of the isotopic composition of the sulfur. Dark colored, fresh glass spherules were analyzed for comparison from a spherulitic bed in the Beloc 1 section that correlates with MU2. The degassing profiles of this sample are almost completely free of any of the gas species considered, and hence characteristic of tektites.

The EGA curve of the spherule B3-7 shows no SO_2 degassing, but a spontaneous water release in a relatively narrow range (between 1000–1100°C), which is more characteristic for degassing of volcanic glasses; on the contrary, impact-derived glasses (e.g., glassy part of suevites, zhamanshinite) typically lose their low water content over a considerably larger temperature range (Heide, 1974; Stelzner and Heide, 1996). Because EGA curves do not permit an exact quantitative evaluation of the amount of water released, these data do not necessarily conflict with the very low water concentrations measured by Koeberl (1992).

The chondrite normalized REE patterns of the glass spherules analyzed resemble the light REE-enriched patterns (La/Yb = 4.2) described by previous workers (Koeberl and Sigurdsson, 1992), but without the negative Eu anomaly found by Koeberl (1993). The REE concentrations in the yellow glass are slightly lower (Fig. 14B; Table 4). Thus contamination of an andesitic to dacitic glass melt by evaporites or carbonates as described by Sigurdsson et al. (1991a) is probable. The REE pattern of the glass spherules does not provide any firm evidence for a volcanic or impact origin, but it allows us to address the problem of the origin of the smectitic and/or palagonitic spherules that were considered by several authors to represent alteration products of these glassy precursors (e.g., Kring and Boynton, 1991; Sigurdsson et al., 1991a; Koeberl and Sigurdsson, 1992; Bohor and Glass, 1995).

In the Beloc 3 section two types of smectites (or palagonites, as defined in Lyons and Officer, 1992; Bohor and Glass, 1995) can be distinguished morphologically: (1) smectite as coatings of glass spherules and (2) smectite spherules as pseudomorphs of impactites, like those described by Izett (1991). These two types also differ significantly in their chemistry. Compared to black and yellow Haiti glass, elements that can be mobilized by alteration are depleted in both types. Na_2O and CaO are nearly completely removed, while SiO_2, K_2O, FeO, and Al_2O_3 are only partly remobilized. Similar element losses were reported in the palagonitized rims of the Haitian glass spherules (Bohor and Glass, 1995). Palagonite is considered to be an incipient phase in the alteration of glass, with a considerably higher Si/Al ratio compared to smectites, into which they transform over time. TiO_2 is immobile during alteration, as are REEs, to a lesser degree. Nevertheless, the smectite spherules are strongly depleted in TiO_2 and REEs relative to both types of glasses, whereas the coatings are TiO_2 enriched by ~20 wt%, compared to the glass nucleus. Although there is increasing evidence that REEs can be efficiently removed during hydrothermal alteration (e.g., Hopf, 1993; Bach and Irber, 1998; Christidis, 1998), the shape of the chondrite-normalized pattern should remain unchanged (Sigurdsson et al., 1991a; Guy et al., 1999). Therefore, even if the low REE contents of the smectite spherules could be attributed to alteration and leaching under a continental weathering regime, implying very high water/rock ratios, the explanation of the positive Eu anomaly in the pattern of the altered spherule analyzed is still not straightforward, and it would be even more problematic to interpret if we consider the negative Eu anomalies of the glass analyzed by Koeberl (1993). Leaching experiments (Bach and Irber, 1998) with hydrothermally altered diabase (to 50% lower REE concentrations than the surrounding, weakly altered rocks) showed significant losses of REE and yielded leaching solutions with negative Eu anomalies compared to the host rock. Nevertheless, the derivation of the smectite spherules from the types of glass material already known is not convincing because the loss of Ti still cannot be readily explained. Thus the smectites probably represent two different genetic types: the smectite coatings are alteration products of the adjacent glass, whereas the smectite spherules, showing very low REE and Ti concentrations, are probably authigenic fillings of voids. None of the glass materials described until now, including the high Si-K glass of Koeberl and Sigurdsson (1992), could have produced by alteration the smectitic spherules analyzed here. In our opinion, the alteration of the glass spherules probably started in the marine sedimentation environment, but may have been completed only after the uplift of the section above sea level, as suggested by Bohor and Glass (1995).

DEPOSITIONAL HISTORY AT BELOC

The age and biostratigraphy of the Beloc section presented here are discussed elsewhere (Keller et al., 2001). The section displays a complex interaction of different sedimentary, volcanic, and cosmogenic sources resulting from a multievent scenario (Fig. 15). The latest Maastrichtian marly limestones indicate a time of relatively high productivity marked by high $\delta^{13}C$ values and high excess rates for Cu, Zn, and Sr, biogenic deposition, and moderately warm temperatures compared with the early Danian. Compared to NASC, REE contents are lower, which is typical for marine carbonates. In particular, NASC-normalized REE patterns show a Ce anomaly, reflecting seawater patterns (Rollinson, 1993). The distribution of the PGEs within the Maastrichtian limestone is similar to that of other marine precipitates (Stüben et al., 2001). Mineralogical bulk-rock data indicate normal pelagic conditions dominated by biogenic calcite, phyllosilicates, opal, and low detrital quartz contents. The presence of hornblende just below the unconformity at the top of the Maastrichtian suggests a volcanic influx due to volcanic activity or to erosion of volcanic rocks.

A spherule-rich deposit marks the earliest Danian *P. eugubina* zone Pla(l) (32–97 cm). The base of the spherule layer of MU1 overlies an undulating erosive surface of the marly limestone enriched in zeolites and amphiboles and marks the paleontologically defined K-T disconformity (e.g., based on the first appearance of Danian species). The spherule-rich deposit is lithologically heterogeneous and is characterized by alternating layers rich in spherules (MU1 and MU2), clayey sediments, and bioclastic limestone. Clasts of reworked Cretaceous sediments are common and suggest intermittent high-energy environments, as indicated by the cross-bedded layer at the top of this interval.

Surface productivity dropped abruptly across this lithological contact and temperatures cooled, as suggested by isotopic data as well as by excess ratios of some trace elements. Due to intensive reworking the entire interval between MU1 and MU3 displays considerable variations in trace element contents, excess ratios, and isotopic data, alternating between values typical for pre-K-T and post-K-T sediments. Detrital minerals are nearly absent here, and this indicates that reworked particles were derived from a pelagic environment (e.g., upper slope), rather than from erosion of an adjacent emerged area.

The cross-bedded layer that marks the top of the high-energy depositional regime of the spherule-rich deposit is overlain by gray-green shale with a thin rust-colored oxidized layer (MU3), which contains the highest values of the Ir-dominated PGE anomaly. Of the PGEs only Ir shows a steady increase from background values in the latest Maastrichtian and the early Danian spherule-rich deposit to 0.6 ng/g in the cross-bedded layer, reaching a maximum of 1 ng/g in the clay and rust-colored layer. The gradual increase in Ir (to 0.6 ng/g) cannot be readily explained by postdepositional remobilization, by decreasing sediment accumulation rates, or by progressive exposure and erosion of an Ir-rich source rock. The Ir anomaly coincides with a possible volcanic influx, as indicated by high zeolite and amphibole contents (Figs. 3 and 8), and decreased calcite content and with drastically lowered sedimentation rates.

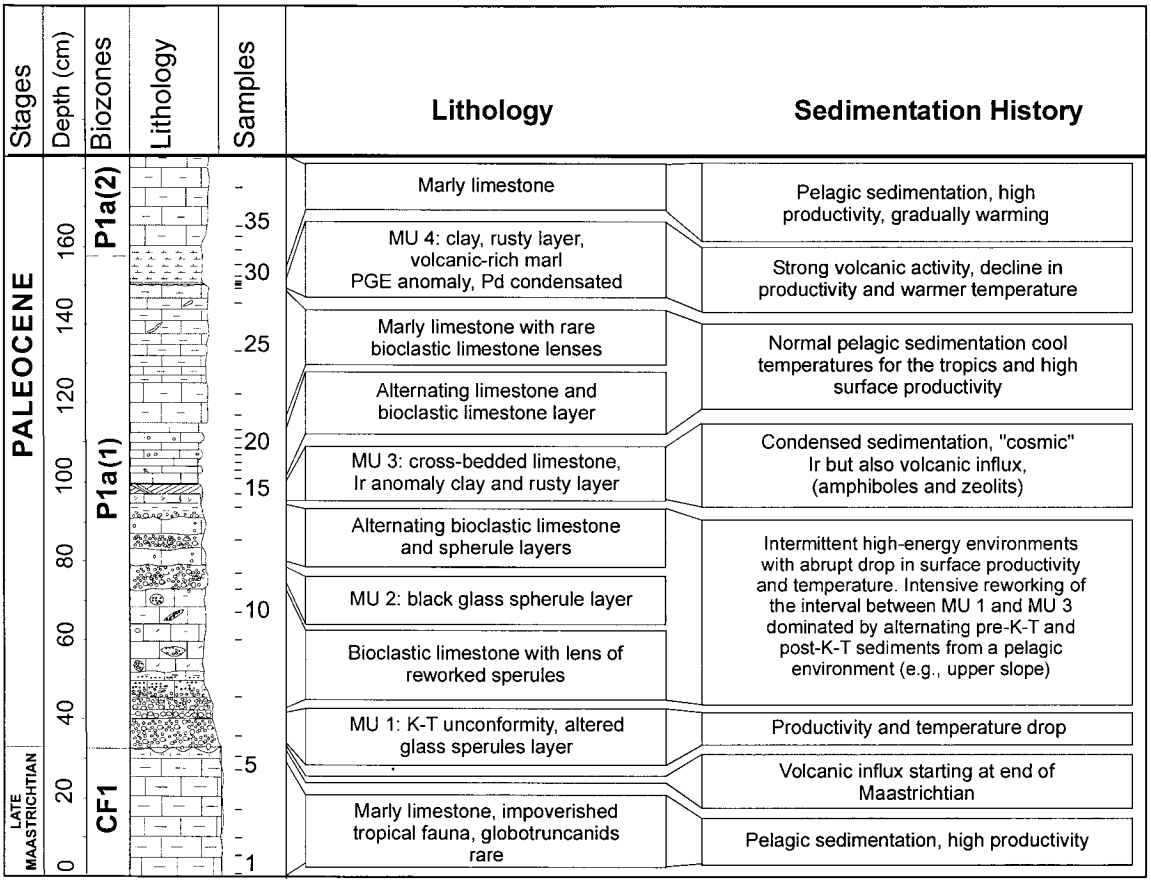

Figure 15. Reconstruction of depositional history of Beloc B3 section based on lithology, mineralogy, sedimentology, and chemostratigraphy. (Lithology, stratigraphy, and biozones are redrawn from Stinnesbeck et al., 1999.) K-T is Cretaceous-Tertiary.

The maximum Ir values within the rust-colored layer (MU3) display a roughly chondritic PGE pattern and may reflect a cosmic overprint on a long-lasting period of volcanic activity. The peak of the Ir anomaly shows a tailing into the surrounding sediments, possibly caused by reworking, diffusion, or bioturbation. The occurrence of glass and smectite spherules below the Ir anomaly may also be considered as indicative of impact material. However, the association of the PGE anomalies with volcanic material (including glass shards) indicates a magmatic contribution and contradicts a pure impact source of the material.

Alternating bioclastic limestones and limestones above the Ir anomaly (105–150 cm, Fig. 8) grade into marly limestones, reflecting normal pelagic sedimentation, as also expressed by carbon and oxygen isotopes and excess values of trace elements. Stable isotopes in this interval indicate very cool temperatures for the tropics and high surface productivity (Fig. 15). This rapid return to nearly pre-K-T values in surface productivity within the lower part of the early Danian zone P1a(1) (lower part of *P. eugubina* zone) is not observed in Tunisian sections (e.g., El Kef) (Keller and Lindinger, 1989), where pre-K-T values are reached in the later Danian zone P1c, but is consistent with low-latitude open-marine environments (Zachos et al., 1989). This may reflect the more stable environment of the Caribbean platform at this time.

Above this interval, MU4 consists of a thin oxidized rust-colored layer and a clay- and clayey marl-layer rich in volcanic glass, amphiboles, and zeolites and is enriched in PGE, particularly in Pd (Fig. 15). The PGE pattern of this anomaly is more compatible with oceanic flood basalts than with a cosmic origin (Greenough and Fryer, 1990). Because Haiti is part of the oceanic flood basalt province within the Caribbean plate, which developed 90 Ma, this PGE anomaly thus may be related with the younger volcanic activity in the Dominican Republic and Costa Rica, which is estimated to have occurred between 69 and 63 Ma (Kerr et al., 1996, 1997; Sinton et al., 1998). Denudation of ultramafic rocks with occasionally very high contents of PGE of middle to Upper Cretaceous age on Jamaica and Tobago (Scott et al., 1999) could also be considered to be responsible for these higher concentrations. Thus, for this anomaly a magmatic origin appears probable. Normalized REE patterns with a strong positive Eu anomaly support this interpretation.

Stable isotope data in MU4 suggest a temporary decline in productivity and warmer temperatures. Above MU4, marly limestones reveal relatively stable high productivity, as also indicated by high calcite contents, C isotopes, and trace element excess rates. Oxygen isotope data show a decreasing trend up to the top of profile, suggesting a gradual warming at that time.

CONCLUSIONS

Detailed geochemical and mineralogical studies of the Beloc section in Haiti revealed the following.

An Ir anomaly is present within a rust-colored clayey layer (MU3) above the spherule-rich deposit. Cosmic and volcanic inputs are reflected by mineral phases, impactites, and chondrite-normalized PGE patterns.

A Pd-dominated PGE anomaly is present 45 cm above the first Ir anomaly and is associated with a second rust-colored layer (MU4) composed of clay, amphiboles, zeolites, and volcanic glass shards. This layer and PGE anomaly are due to volcanic activity, as indicated by mineral composition and chondrite-normalized PGE and REE patterns.

The chemical variations within the three types of spherules found in the lower marker units can be explained by post-depositional alteration and/or by the lithological heterogeneity of the target material.

ACKNOWLEDGMENTS

This study was supported by the Deutsche Forschungsgemeinschaft (grants Sti128/2-1 and Sti128/2-2, and Stu 169/10-1), the National Science Foundation (grant OCE-9021338), the Petroleum Research Fund (grant 2670-AC8), and the Swiss National Fund (grant 8220-028367). We thank Jan Smit and R. Rocchia for reviewing the paper.

REFERENCES CITED

Adatte, T., Stinnesbeck, W., and Keller, G., 1996, Lithostratigraphic and mineralogical correlations of near K/T boundary clastic sediments in northeastern Mexico: Implications for origin and nature of deposition, *in* Ryder, G., Fastovsky, D., and Gartner, S., eds., The Cretaceous-Tertiary event and other catastrophes in Earth history: Geological Society of America Special Paper 307, p. 211–226.

Alvarez, L.W., Alvarez, W., Asaro, F., and Michel, H.V., 1980, Extraterrestrial cause for the Cretaceous-Tertiary extinction experimental results and theoretical interpretation: Science, v. 208, p. 1095–1108.

Alvarez, L.W., Alvarez, W., Asaro, F., and Michel, H.V., 1982, Current status of the impact theory for the terminal Cretaceous extinction, *in* Silver, L.T., and Schultz, P.H., eds., Geological implications of impacts of large asteroids and comets on the Earth: Geological Society of America Special Paper 190, p. 305–315.

Anbar, A.D., Wasserburg, G.J., Papanastassiou, D.A., and Andersson, P.S., 1996, Iridium in natural waters: Science, v. 273, p. 1524–1528.

Andreozzi, M., Dinelli, E., and Tateo, F., 1997, Geochemical and mineralogical criteria for the identification of ash layers in the stratigraphic framework of a foredeep: The early Miocene Mt. Cervarola Sandstones, northern Italy: Chemical Geology, v. 137, p. 23–39.

Bach, W., and Irber, W., 1998, Rare earth element mobility in the oceanic lower sheeted dyke complex: Evidence from geochemical data and leaching experiments: Chemical Geology, v.151, p. 309–326.

Barkatt, A., Boulos, M., Barkatt, A., Samsapour, W., Boroomand, M., and Macedo, P., 1984, The chemical durability of tektites laboratory study and correlation with long-term corrosion behaviour: Geochimica et Cosmochimica Acta, v. 48, p. 361–371.

Blum, J.D., and Chamberlain, C.P., 1992, Oxygen isotope constraints on the origin of impact glasses from the Cretaceous-Tertiary boundary: Science, v. 257, p. 1104–1107.

Blum, J.D., Chamberlain, C.P., Hingston, M.P., Koeberl, C., Marin, L.E., Schuraytz, B.C., and Sharpton, V.L., 1993, Isotopic comparison of K/T boundary impact glass with melt rock from the Chicxulub and Manson structures: Nature, v. 364, p. 325–327.

Bohor, B.F., and Glass, B.P., 1995, Origin and diagenesis of K/T impact spherules: From Haiti to Wyoming and beyond: Meteoritics, v. 30, p. 182–198.

Bohor, B.F., and Seitz, R., 1990, Cuban K/T catastrophe: Nature, v. 433, p. 593.

Borg, G., Tredoux, M., Maiden, K., Sellschop, J., and Wayward, O., 1987, PGE- and Au-distribution in rift-related volcanics, sediments and strata-bound Cu/Ag ores of middle Proterozoic age in Central SWA/ Namibia, *in* Prichard, H., Potts, P., Bowles, J., and Cribb, S., eds., Geo-Platinum 87: London and New York, Elsevier, p. 303–317.

Bowles, J.F.W., 1986, The development of platinum-group minerals in laterites: Economic Geology, v. 81, p. 1278–1285.

Chaussidon, M., Sigurdsson, H., and Métrich, N., 1996, Sulfur and boron isotope study of high-Ca impact glasses from the K/T boundary: Constraints on source rocks, *in* Ryder, G., Fastovsky, D., and Gartner, S., eds., The Cretaceous-Tertiary event and other catastrophes in Earth history: Geological Society of America Special Paper 307, p. 253–262.

Christidis, G.E., 1998, Comparative study of the mobility of major and trace elements during alteration of an andesite and rhyolite to bentonite in the islands of Milos and Kimolos, Aegean, Greece: Clays and Clay Minerals, v. 46, p. 379–399.

Colodner, D.C., Boyle, E.A., Edmond, J.M., and Thomson, J., 1992, Post-depositional mobility of platinum, iridium, and rhenium in marine sediments: Nature, v. 358, p. 402–404.

Condie, K.C., 1991, Another look at rare earth elements in shales: Geochimica et Cosmochimica Acta, v. 55, p. 2527–2531.

Crocket, J., and Kabir, A., 1988, PGE in Hawaiian basalt: Implication of hydrothermal alteration on PGE mobility in volcanic fluids, *in* Prichard, H., Potts, P., Bowles, J., and Cribb, S., eds., Geoplatinum: London and New York, Elsevier, p. 259.

Crocket, J.H., Officer, C.B., Wezel, F.C., and Johnson, G.D., 1988, Distribution of noble metals across the Cretaceous/Tertiary boundary at Gubbio, Italy: Iridium variation as a constraint on the duration and nature of Cretaceous/Tertiary boundary events: Geology, v. 16, p. 77–88.

Dai, X., Chai, Z., Mao, X., and Ouyang, H., 2000, Sorption and desorption of iridium by coastal sediment: Effects of iridium speciation and sediment components: Chemical Geology, v. 166, p. 15–22.

Date, A.R., Davis, A.E., and Cheung, Y.Y., 1987, The potential of fire assay and inductively coupled plasma source mass spectrometry for the determination of platinum group elements in geological materials: Analyst, v. 112, p. 1217–1222.

Deer, W.A, Howie, R.A., and Zussman, J., 1992, An introduction to the rock-forming minerals (second edition): London, Longman Scientific and Technical, 696 p.

Dyer, B.D., Lyalikova, N.N., Murray, D., Doyle, M., Kolesov, G.M., and Krumbein, W., 1989, Role for microorganisms in the formation of iridium anomalies: Geology, v. 17, p. 1036–1039.

Elderfield, H., and Greaves, M.J., 1982, The rare earth elements in seawater: Nature, v. 296, p. 214–219.

Elliot, W.C., 1993, Origin of the Mg-smectite at the Cretaceous/Tertiary (K/T) boundary at Stevns Klint, Denmark: Clays and Clay Minerals, v. 41, p. 442–452.

Evans, N.J., and Chai, C.F., 1997, The distribution and geochemistry of platinum-group elements as event markers in the Phanerozoic: Palaeogeography, Palaeoclimatology, Palaeoecology, v. 132, p. 373–390.

Evans, D.M., Buchanan, D.L., and Hall, G.E.M., 1994, Dispersion of platinum, palladium and gold from the main sulphide zone, Great Dyke, Zimbabwe: Institution of Mining and Metallurgy, Transactions, Section B: Applied Earth Science, v. 103, p. B57–B67.

Evans, N.J., Ahrens, T.J., and Gregoire, D.C., 1995, Fractionation of ruthenium from iridium at the Cretaceous-Tertiary boundary: Earth and Planetary Science Letters, v. 134, p. 141–153.

Fleet, A.J., 1984, Aqueous and sedimentary geochemistry of the rare earth elements, *in* Henderson, P., ed., Rare earth element geochemistry: Amsterdam, Elsevier, Developments in Geochemistry 2, p. 343–373.

Ganapathy, R., 1980, A major meteorite impact on the Earth 65 million years ago: Evidence from the Cretaceous-Tertiary boundary clay: Science, v. 209, p. 921–923.

Glasby, G.P., and Kunzendorf, H., 1996, Multiple factors in the origin of the Cretaceous/Tertiary boundary: The role of environmental stress and Deccan Trap volcanism: Geologische Rundschau, v. 85, p.191–210.

Greenough, J.D., and Fryer, B.J., 1990, Indian Ocean basalts, *in* Duncan, R.A., and Backmann, J., et al., eds., Proceedings of the Ocean Drilling Program, Scientific Results, Leg 115: College Station, Texas, Ocean Drilling Program, p. 71–84.

Gromet, L.P., Dymek, R.F., Haskin, L.A., and Korotev, R.L., 1984, The "North American shale composite": Its compilation, major and trace element characteristics: Geochimica et Cosmochimica Acta, v. 48, p. 2469–2482.

Guy, C., Daux, V., and Schott, J., 1999, Behaviour of rare earth elements during seawater/basalt interactions in the Mururoa Massif: Chemical Geology, v. 158, p. 21–35.

Hannigan, R., and Basu, A.R., 1998, Late diagenetic trace element remobilization in organic-rich black shales of the Taconic Foreland Basin of Québec, Ontario and New York, *in* Schieber, J., Zimmerle, W., and Sethi, P.S., eds., Shales and mudstones 2: Stuttgart, Germany, Schweizerbart'sche Verlagsbuchhandlung (Nägele u. Obermüller), Petrography, Petrophysics, Geochemistry, and Economic Geology, p. 209–234.

Hataway, J.C., and Sachs, P.L., 1965, Sepiolite and clinoptilolite from the mid-Atlantic Ridge: American Mineralogist, v. 50, p. 852–867.

Heide, K., 1974, Untersuchung der Hochvakuumentgasung bei dynamischer Temperaturänderung bis 1200°C von natürlichen Gläsern unterschiedlicher Genese: Chemie der Erde, v. 33, p. 195–214.

Hildebrand, A.R., Penfield, G.T., Kring, D.A., Pilkington, M., Camargo, A., Jacobson, Z.S.B., and Channell, J.E.T., 1991, Glass from the Cretaceous/Tertiary boundary in Haiti: Nature, v. 349, p. 482.

Hildebrand, A.R., and Boyton, W.V., 1990, Proximal Cretaceous-Tertiary boundary impact deposits in the Caribbean: Science, v. 248, p. 843.

Hopf, S., 1993, Behaviour of rare earth elements in geothermal systems of New Zealand: Journal of Geochemical Exploration, v. 47, p. 333–357.

Hu, X., Wang, Y.L., and Schmitt, R.A., 1988, Geochemistry of sediments on the Rio Grande Rise and the redox evolution of the South Atlantic Ocean: Geochimica et Cosmochimica Acta, v. 52, p. 201–207.

Izett, G.A., 1991, Tektites in Cretaceous-Tertiary boundary rocks on Haiti and their bearing on the Alvarez impact extinction hypothesis: Journal of Geophysical Research, v. 96, p. 20879–20905.

Izett, G.A., Maurrasse, F.J.-M.R., Lichte, F.E., Meeker, G.P., and Bates, R., 1990, Tektites in Cretaceous-Tertiary boundary rocks on Haiti: U.S. Geological Survey Open-File Report 90–635, 31 p.

Izett, G.A., Dalrymple, G.B., and Snee, L.W., 1991, $^{40}Ar/^{39}Ar$ age of Cretaceous/Tertiary boundary tektites from Haiti: Science, v. 252, p. 1539–1542.

Jéhanno, C., Boclet, D., Froget, L., Lambert, B., Robin, E., Rocchia, R., and Turpin, L., 1992, The Cretaceous-Tertiary boundary at Beloc, Haiti: No evidence for an impact in the Caribbean area: Earth and Planetary Science Letters, v. 109, p. 229–241.

Jenkyns, H.C., Gale, A.S., and Corfield, R.M., 1994, Carbon- and oxygen-isotope stratigraphy of the English Chalk and Italian Scaglia and its paleoclimatic significance: Geological Magazine, v. 131, p. 1–34.

Kastner, M., and Stonecipher, S.A., 1978, Zeolites in pelagic sediments of the Atlantic, Pacific and Indian Oceans, *in* Sand, L.B., and Mumpton, F.A., eds., Natural zeolithes occurrence, properties, use: Oxford, Pergamon Press, p. 199–220.

Keller, G., and Lindinger, M., 1989, Stable isotope, TOC and $CaCO_3$ record across the Cretaceous/Tertiary boundary at El Kef, Tunisia: Palaeogeography, Palaeoclimatology, Palaeoecology, v. 73, p. 243–265.

Keller, G., and Stinnesbeck, W., 1996, Sea level changes, clastic deposits and megatsunamis across the Cretaceous/Tertiary boundary, *in* MacLeod, N., and Keller, G., eds., The Cretaceous-Tertiary boundary mass extinction: Biotic and environmental events: New York, Norton Press, p. 415–449.

Keller, G., Lopez-Oliva, J.G., Stinnesbeck, W., and Adatte, T., 1997, Age, stratigraphy and deposition of near K/T siliciclastic deposits in Mexico: Relation to bolide impact?: Geological Society of America Bulletin, v. 109, p. 410–428.

Keller, G., Adatte, T., Stinnesbeck, W., Stüben, D., and Berner, Z., 2001, Age, chemo- and biostratigraphy of Haiti spherule-rich deposits: A multi-event K-T scenario: Canadian Journal of Earth Sciences, v. 38, p. 197–227.

Kerr, A.C., Tarney, J., Marriner, G.F., Nivia, A., Klaver, G.T., and Saunders, A.D., 1996, The geochemistry and tectonic setting of late Cretaceous Caribbean and Colombian volcanism: Journal of South American Earth Sciences, v. 9, p. 111–120.

Kerr, A.C., Marriner, G.F., Tarney, J., Nivia, A., Saunders, A.D., Thirlwall, M.F., and Sinton, C.W., 1997, Cretaceous basaltic terranes in western Colombia: Elemental, chronological and Sr-Nd isotopic constraints on petrogenesis: Journal of Petrology, v. 38, p. 677–702.

Killingley, J.S., 1983, Effects of diagenetic recrystallization on $^{18}O/^{16}O$ values of deep-sea sediments: Nature, v. 301, p. 594–597.

Klug, H.P., and Alexander, L., 1974, X-ray diffraction procedures for polycrystalline and amorphous materials (first and second editions): New York, John Wiley and Sons, 960 p.

Koeberl, C., 1992, Water content of glasses from the K/T boundary, Haiti: An indication of impact origin: Geochimica et Cosmochimica Acta, v. 56, p. 4329–4332.

Koeberl, C., 1993, Chicxulub Crater, Yucatan: Tektites, impact glasses, and the geochemistry of target rocks and breccias: Geology, v. 21, p. 211–214.

Koeberl, C., and Sigurdsson, H., 1992, Geochemistry of impact glasses from the K/T boundary in Haiti: Relation to smectites and new types of glass: Geochimica et Cosmochimica Acta, v. 56, p. 2113–2129.

Koeberl, C., Sharpton, V.L., Schuraytz, B.C., Shirey, S.B., Blum, J.D., and Marin, L.E., 1994, Evidence for a meteoritic component in impact melt rock from the Chicxulub structure: Geochimica et Cosmochimica Acta, v. 58, p. 1679–1884.

Kramar, U., 1997, Advances in energy-dispersive x-ray fluorescence: Journal of Geochemical Exploration, v. 58, p. 73–80.

Kring, D.A., and Boynton, W.V., 1991, Altered spherules of impact melt and associated relic glass from the K/T boundary sediments in Haiti: Geochimica et Cosmochimica Acta, v. 55, p. 1737–1742.

Kring, D.A., Hildebrand, A.R., and Boynton, W.V., 1994, Provenance of mineral phases in the Cretaceous-Tertiary boundary sediments exposed on the southern peninsula of Haiti: Earth and Planetary Science Letters, v. 128, p. 629–641.

Kübler, B., 1983, Dosage quantitatif des minéraux majeurs des roches sédimentaires par diffraction X: Cahier de l'Institut de Géologie de Neuchatel, Suisse, sér. ADX, 1.1 and 1.2, 15 p.

Kübler, B., 1987, Cristallinité de l'illite, méthodes normalisées de préparations, méthodes normalisées de mesures: Cahiers de l'Institut de Géologie de Neuchatel, Suisse, sér. ADX, 3, 21 p.

Kyte, F.T., Zhiming, Z., and Wasson, J.T., 1980, Siderophile-enriched sedi-

ments from the Cretaceous-Tertiary boundary: Nature, v. 288, p. 651–656.

Kyte, F.T., Bostwick, J.A., and Zhou, L., 1996, The Cretaceous-Tertiary boundary on the Pacific plate: Composition and distribution of impact debris, *in* Ryder, G., Fastovsky, D., and Gartner, S., eds., The Cretaceous-Tertiary event and other catastrophes in Earth history: Geological Society of America Special Paper 307, p. 389–401.

Lamolda, M., Aguado, R., Maurrasse, F.T.-M.R., and Peryt, D., 1997, El transito Cretacico–Terciario en Beloc, Haiti: Registro micropaleontológico e implicaciones bioestratigraficas: Geogaceta, v. 22, p. 97–100.

Leinen, M., and Stakes, D., 1979, Metal accumulation rate in the central Pacific during Cenozoic time: Geological Society of America Bulletin, v. 90, p. 357–375.

Leinen, M., Cwienk, D., Heath, G.R., Biscaye, P.E., Kolla, V., Thiede J., and Dauphin, J.P., 1986, Distribution of biogenic silica and quartz in recent deep-sea sediments: Geology, v. 14, p. 199–203.

Lerbekmo, J.F., Sweet, A.R., and Davidson, R.A., 1999, Geochemistry of the Cretaceous–Tertiary (K-T) boundary interval: South-central Saskatchewan and Montana: Canadian Journal of Earth Sciences, v. 36, p. 717–724.

Leroux, H., Rocchia, R., Froget, L., Orue-Etxebarria, X., Doukhan, J., and Robin, E., 1995, The K/T boundary of Beloc (Haiti): Compared stratigraphic distributions of boundary markers: Earth and Planetary Science Letters, v. 131, p. 255–268.

Li, L., Keller, G., Adatte, T., and Stinnesbeck, W., 2001, Late Cretaceous sea level changes in Tunisia: A multi-disciplinary approach: Journal of the Geological Society [London] v. 157, p. 447–458.

Lyons, J.B., and Officer, C.B., 1992, Mineralogy and petrology of the Haiti Cretaceous/Tertiary section: Earth and Planetary Science Letters, v. 109, p. 205–224.

MacRae, N.D., Nesbitt, H.W., and Kronberg, B.I., 1992, Development of a positive Eu anomaly during diagenesis: Earth and Planetary Science Letters, v. 109, p. 585–591.

Martin-Barajas, A., and Lallier-Verges, E., 1993, Ash layers and pumice in the central Indian basin: Relationship to the formation of manganese nodules: Marine Geology, v. 115, p. 307–329.

Maurrasse, F.J.-M.R., 1982, Survey of the geology of Haiti, *in* Guide to the field excursions in Haiti: Miami, Florida, Miami Geological Society, v. 130, 103 p.

Maurrasse, F.J.-M.R., and Sen, G., 1991, Impacts, tsunamis, and the Haitian Cretaceous-Tertiary boundary layer: Science, v. 252, p. 1690–1693.

McDonough, W.F., and Sun, S.-S., 1995, The composition of the earth: Chemical Geology, v. 120, p. 223–253.

McLennan, S.M., 1989, Rare earth elements in sedimentary rocks: Influence of provenance and sedimentary processes, *in* Lipin, B.R., and McKay, G.A., eds., Geochemistry and mineralogy of rare earth elements: Washington, D.C., Mineralogical Society of America, Reviews in Mineralogy, v. 21, p. 169–200.

Mitchell, S.F., Ball, J.D., Crowley, S.F., Marshall, J.D., Paul, C.R.C., Veltkamp, C.J., and Samir, A., 1997, Isotope data from cretaceous chalks and foraminifera: Environmental or diagenetic signals?: Geology, v. 25, p. 691–694.

Montanari, A., and Koeberl, C., 2000, Impact stratigraphy: Heidelberg, Germany, Springer-Verlag, 364 p.

Murray, R.W., and Leinen, M., 1993, Chemical transport to the seafloor of the equatorial Pacific Ocean across a latitudinal transect at 135° W: Tracking sedimentary major, trace and rare earth element fluxes at the equator and the Intertropical Convergence Zone: Geochimica et Cosmochimica Acta, v. 57, p. 4141–4163.

Murray, R.W., and Leinen, M., 1996, Scavenged excess aluminum and its relationship to bulk titanium in biogenic sediment from central equatorial Pacific Ocean: Geochimica et Cosmochimica Acta, v. 60, p. 3869–3878.

Murray, R.W., Buchholtz ten Brink, M.R., Jones, D.L., Gerlach, D.C., and Russ G.P., III, 1990, Rare earth elements as indicators of different marine depositional environment in chert and shale: Geology, v. 18, p. 268–293.

Officer, C.B., and Drake, C.L., 1985, Terminal Cretaceous environmental events: Science, v. 277, p. 1161–1167.

Ohr, M., Halliday, A.N., and Peacor, D.R., 1994, Mobility and fractionation of rare earth elements in argillaceous sediments: Implications for dating diagenesis and low-grade metamorphism: Geochimica et Cosmochimica Acta, v. 58, p. 289–312.

Orians, K.J., Boyle, E.A., and Bruland, K.W., 1990, Dissolved titanium in the open ocean: Nature, v. 348, p. 322–325.

Orth, C.J., Quintana, L.R., Gilmore, J.S., Barrick, J.E., Haywa, J.N., and Speshardt, S.A., 1988, Pt-metal anomalies in the lower Mississippian of southern Oklahoma: Geology, v. 16, p. 627–603.

Palmer, M.R., 1985, Rare earth elements in foraminifera tests: Earth and Planetary Science Letters, v. 73, p. 285–298.

Pattan, J.N., Rao, Ch.M., Higgs, N.C., Colley, S., and Parthiban, G., 1995, Distribution of major, trace and rare-earth elements in surface sediments of the Wharton Basin, Indian Ocean: Chemical Geology, v. 121, p. 201–215.

Reddi, G.S., Rao, C.R.M., Rao, T.A.S, Lakshmi, S.V., Prabhu, R.K., and Mahalingam, T.R., 1994, Nickel sulphide fire assay: ICPMS method for the determination of platinum group elements—A detailed study on the recovery and losses at different stages: Fresenius Journal of Analytical Chemistry, v. 348, p. 350–352.

Rocchia, R., and Robin, E., 1998, The stratigraphic distribution of iridium at the Cretaceous–Tertiary boundary of El Kef, Tunisia: Bulletin de la Société Géologique de France, v. 169, p. 515–526.

Rocchia, R., Boclet, D., Bonté, Ph., Jéhanno, C., Chen, Y., Courtillot, V., Mary, C., and Wezel, F., 1990, The Cretaceous-Tertiary boundary at Gubbio revisited: Vertical extent of the Ir anomaly: Earth and Planetary Science Letters, v. 99, p. 206–219.

Rocchia, E., Robin, E., Froget, L., and Gayraud, J., 1996, Stratigraphic distribution of extraterrestrial markers at the Cretaceous-Tertiary boundary in the Gulf of Mexico area: Implications for the temporal complexity of the event, *in* Ryder, G., Fastovsky, D., and Gartner, S., eds., The Cretaceous-Tertiary event and other catastrophes in Earth history: Geological Society of America Special Paper 307, p. 279–302.

Rock, N.M.S., 1988, Numerical geology: Berlin, Springer-Verlag, Lecture Notes in Earth Sciences, v. 18, 427 p.

Rollinson, H., 1993, Using geochemical data: London, Longman, 352 p.

Sawlowicz, Z., 1993, Iridium and other platinum-group elements as geochemical markers in sedimentary environments: Palaeogeography, Palaeoclimatology, Palaeoecology, v. 104, p. 253–270.

Schrag, D.P., DePaolo, D.J., and Richter, F.M., 1995, Reconstructing past sea surface temperatures: Correcting for diagenesis of bulk marine carbonate: Geochimica et Cosmochimica Acta, v. 59, p. 2265–2278.

Schroeder, J.O., Murray, R.W., Leinen, M., Pflaum, R.C., and Janacek, T.R., 1997, Barium in equatorial Pacific carbonate sediment: Terrigenous, oxide, and biogenic associations: Paleoceanography, v. 12, no. 1, p. 125–146.

Scott, P.W., Jackson, T.A., and Dunham, A.C., 1999, Economic potential of the ultramafic rocks of Jamaica and Tobago: Two contrasting geological settings in the Caribbean: Mineralium Deposita, v. 34, p. 718–723.

Sethi, P.S., Hanningan, R.E., and Leithold, E.L., 1998, Rare-earth element chemistry of Cenomanian-Turonian shales of the North American Greenhorn Sea, Utah, *in* Schieber, J., Zimmerle, W., and Sethi, P.S., eds., Shales and mudstones: Stuttgart, Germany, Schweizerbart'sche Verlagsbuchhandlung (Nägele u. Obermüller), p. 195–208.

Shields, G., and Stille, P., 1998, Stratigraphic trends in cerium anomaly in authigenic marine carbonates and phosphates: Diagenetic alteration or seawater signals? [abs.]: Goldschmidt Conference, Toulouse, Mineralogical Magazine, v. 62A, p. 1387–1388.

Sigurdsson, H., D'Hondt, S., Arthur, M.A., Bralower, T.J., Zachos, J.C., Van Fossen, M., and Channell, J.E.T., 1991a, Glass from the Cretaceous/Tertiary boundary in Haiti: Nature, v. 349, p. 482–487.

Sigurdsson, H., Bonté, Ph., Turpin, L., Chaussidon, M., Metrich, N., Steinberg,

M., Pradel, Ph., and D'Hondt, S.D., 1991b, Geochemical constraints on source region of Cretaceous/Tertiary impact glasses: Nature, v. 353, p. 839–842.

Sinton, C.W., Duncan, R.A., Storey, M., Lewis, J., and Estrada, J.J., 1998, An oceanic flood basalt province within the Caribbean plate: Earth and Planetary Science Letters, v. 155, p. 221–235.

Smit, J., 1999, The global stratigraphy of the Cretaceous-Tertiary boundary impact ejecta: Annual Reviews in Earth and Planetary Science, v. 27, p. 75–113.

Smit, J., Montanari, A., Swinburne, N.H.M., Alvarez, W., Hildebrand, A., Margolis, S.V., Claeys, P., Lowrie, W., and Asaro, F., 1992, Tektite-bearing deep-water clastic unit at the Cretaceous-Tertiary boundary in northeastern Mexico: Geology, v. 20, p. 99–103.

Stelzner, Th., and Heide, K., 1996, The study of weathering products of meteorites by means of evolved gas analysis: Meteoritics and Planetary Science, v. 31, p. 249–254.

Stinnesbeck, W., Barbarin, J.M., Keller, G., Lopez-Oliva, J.G., Pivnik, D., Lyons, J., Officer, C., Adatte, T., Graup, G., Rocchia, R., and Robin, E., 1993, Deposition of channel deposits near the Cretaceous/Tertiary boundary in northeastern Mexico: Catastrophic or "normal" sedimentary deposits?: Geology, v. 21, p. 797–800.

Stinnesbeck, W., Keller, G., Adatte, T., Stüben, D., Kramar, U., Berner, Z., Desremeaux, C., and Molière, E., 1999, Beloc, Haiti, revisited: Multiple events across the Cretaceous-Tertiary transition in the Caribbean: Terra Nova, v. 11, p. 303–310.

Stinnesbeck, W., Schulte, P., Lindenmaier, F., Adatte, T., Affolter, M., Schilli, L., Keller, G., Stüben, D., Berner, Z., Kramar, U., Burns, S., and Lopez-Oliva, J.G., 2001, Late Maastrichtian age of spherule deposits in northeastern Mexico: Implication for Chicxulub scenario: Canadian Journal of Earth Sciences, v. 38, p. 1–10.

Stoll, H.M., and Schrag, D.P., 1996, Evidence for glacial control of rapid sea level changes in the Early Cretaceous: Science, v. 272, p. 1171–1174.

Stoll, H.M., and Schrag, D.P., 1998, Effects of Quaternary sea level cycles on strontium in seawater: Geochimica et Cosmochimica Acta, v. 62, p. 1107–1118.

Stüben, D., Glasby, G.P., Eckhardt, J.-D., Berner, Z., Mountain, B.W., and Usui, A., 1999, Enrichments of platinum-group elements in hydrogeneous, diagenetic and hydrothermal marine manganese and iron deposits: Exploration and Mining Geology, v. 8, p. 1–15.

Stüben, D., Kramar, U., Berner, Z., Stinnesbeck, W., Keller, G., and Adatte, T., 2001, Trace elements, stable isotopes, and clay mineralogy of the Elles II K/T profile: Indications for sealevel fluctuations and primary productivity: Palaeogeography, Palaeoclimatology, Palaeoecology, special volumne (in press).

Sutherland, F.L., 1994, Volcanism around K/T boundary time: Its role in an impact scenario for the K/T extinction event: Earth Science Reviews, v. 36, p. 1–26.

Taylor, S.R., and McLennan, S.M., 1985, The continental crust: Its composition and evolution: Oxford, Blackwell, 312 p.

Terakado, Y., and Nakajima, W., 1995, Characteristics of rare-earth elements, Ba, Sr and Rb abundances in natural zeolithes: Geochemical Journal, v. 29, p. 337–345.

Torres, M.E., Brumsack, H.J., Bohrmann, G., and Emeis, K.C., 1996, Barite fronts in continental margin sediments: A new look at barium remobilization in the zone of sulfate reduction and formation of heavy barites in diagenetic fronts: Chemical Geology, v. 127, p. 125–139.

Tredoux, M., DeWitt, M.J., Hart, R.J., Lindsay, N.M., Verhagen, B., and Sellschop, J.P.F., 1989, Chemostratigraphy across the Cretaceous-Tertiary boundary and a critical assessment of the iridium anomaly: Journal of Geology, v. 97, p. 585–605.

Wallace, M.W., Gostin, V.A., and Keays, R.R., 1990, Acraman impact ejecta and host shales: Evidence for low-temperature mobilization of iridium and other platinoids: Geology, v. 18, p. 132–135.

Weaver, C.E., 1968, Mineral facies in the Tertiary of the continental shelf and Blake Plateau: Southeastern Geology, v. 9, p. 57–63.

Westland, A.D., 1981, Inorganic chemistry of the platinum-group elements, *in* Cabri, L.J., ed., Platinum-group elements: Mineralogy, geology and recovery: Canadian Institute of Mining and Metallurgy, Special Issue, v. 23, p. 5–18.

Winter, B.L., Johnson, C.M., Clark, D.L., 1997, Geochemical constraints on the formation of Late Cenozoic ferromanganese micronodules from the central Arctic Ocean: Marine Geology, v. 138, p. 149–169.

Zachos, J.C., Arthur, M.A., Thunell, R.C., Williams, D.F., and Tappa, E.J., 1985, Stable isotope and trace element geochemistry of carbonate sediments across the Cretaceous/Tertiary boundary at Deep Sea Drilling Project Hole 577, Leg 86, *in* Heath, G.R., Burckle, L.H., et al., eds, Initial reports of the Deep Sea Drilling Project, Volume 86: Washington, D.C., U.S. Government Printing Office, p. 513–532.

Zachos, J.C., Arthur, M.A., and Dean, W.E., 1989, Geochemical evidence for suppression of pelagic marine productivity at the Cretaceous/Tertiary boundary: Nature, v. 337, p. 61–64.

Zereini, F., Skerstupp, B., and Urban, H., 1994, Comparison between the use of sodium and lithium tetraborate in platinum-group element determination by nickel sulphide fire-assay: Geostandards Newsletter, v. 18, p. 105–109.

Zielinski, R.A., 1982, The mobility of uranium and other elements during alteration of rhyolite ash to montmorilonite: A case study in the Troublesome Formation, Colorado, U.S.A.: Chemical Geology, v. 35, p. 185–204.

Zielinski, R.A., 1985, Element mobility during alteration of silicic ash to kaolinite: A study of tonstein: Sedimentology, v. 32, p. 567–579.

Manuscript Submitted October 10, 2000; Accepted by the Society March 22, 2001